Light Stable Isotopes (H, B, C, O and S) in Ore Studies—Methods, Theory, Applications and Uncertainties

David L. Huston , Robert B. Trumbull, Georges Beaudoin, and Trevor Ireland

Abstract

Variations in the abundances of light stable isotopes, particularly those of hydrogen, boron, carbon, oxygen and sulfur, were essential in developing mineralization models. The data provide constraints on sources of hydrothermal fluids, carbon, boron and sulfur, track interaction of these fluids with the rocks at both the deposit and district scales, and establish processes of ore deposition. In providing such constraints, isotopic data have been integral in developing genetic models for porphyry-epithermal, volcanic-hosted massive sulfide, orogenic gold, sediment-hosted base metal and banded-iron formation-hosted iron ore systems, as discussed here and in other chapters

D. L. Huston (✉)
Geoscience Australia, GPO Box 378, Canberra, ACT 2601, Australia
e-mail: David.Huston@ga.gov.au

R. B. Trumbull
Helmholtz Centre Potsdam, GFZ German Research Centre for Geosciences, Telegrafenberg B125, Potsdam 14473, Germany

G. Beaudoin
Département de Géologie et de Génie Géologique, Université Laval, 1065, Avenue de La Médecine, Québec, QC G1V 0A6, Canada

T. Ireland
School of Earth and Environmental Sciences, University of Queensland, St Lucia, QLD 4072, Australia

in this book. After providing conventions, definitions and standards used to present stable isotope data, this chapter summarizes analytical methods, both bulk and in situ, discusses processes that fractionate stable isotopes, documents the isotopic characteristics of major fluid and rock reservoirs, and then shows how stable isotope data have been used to better understand ore-forming processes and to provide vectors to ore. Analytical procedures, initially developed in the 1940s for carbon–oxygen analysis of bulk samples of carbonate minerals, have developed so that, for most stable isotopic systems, spots as small as a few tens of μm are routinely analyzed. This precision provides the paragenetic and spatial resolution necessary to answer previously unresolvable genetic questions (and create new questions). Stable isotope fractionation reflects geological and geochemical processes important in ore formation, including: (1) phase changes such as boiling, (2) water–rock interaction, (3) cooling, (4) fluid mixing, (5) devolatilization, and (6) redox reactions, including SO_2 disproportionation caused by the cooling of magmatic-hydrothermal fluids and photolytic dissociation in the atmosphere. These processes commonly produce gradients in isotopic data, both in time and in space. These gradients, commonly mappable in space, provide not only evidence of process but also exploration vectors. Stable isotope data can be used to estimate the conditions of alteration or

mineralization when data for coexisting minerals are available. These estimates use experimentally- or theoretically-determined fractionation equations to estimate temperatures of mineral formation. If the temperature is known from isotopic or other data (e.g., fluid inclusion data or chemical geothermometers), the isotopic composition of the hydrothermal fluid components can be estimated. If fluid inclusion homogenization and compositional data exist, the pressure and depth of mineralization can be estimated. One of the most common uses of stable isotope data has been to determine, or more correctly delimit, fluid and sulfur sources. Estimates of the isotopic compositions of hydrothermal fluids, in most cases, do not define unequivocal sources, but, rather, eliminate sources. As an example, the field of magmatic fluids largely overlap that of metamorphic fluids in $\delta^{18}O$-δD space, but are significantly different to the fields of meteoric waters and seawater. As such, a meteoric or seawater origin for a fluid source may be resolvable, but a magmatic source cannot be resolved from a metamorphic source. Similarly, although $\delta^{34}S \sim 0$‰ is consistent with a magmatic-hydrothermal sulfur source, the signature can also be produced by leaching of an igneous source. Recent analytical and conceptual advances have enabled gathering of new types of isotopic data and application of these data to resolve new problems in mineral deposit genesis and geosciences in general. Recent developments such as rapid isotopic analysis of geological materials or clumped isotopes will continue to increase the utility of stable isotope data in mineral deposit genesis and metallogeny, and, importantly, for mineral exploration.

1   Introduction

In the early 1900s isotopes, which are now recognized as atoms of a chemical element that differ in the number of neutrons, were discovered independently by studying radioactive decay series (Soddy 1913) and measuring the deflection of neon ions through a magnetic field (Thomson 1913). In the case of radioactive isotopes, different isotopes were originally described as different elements, however, both of these investigations concluded that there were varieties of chemical elements, which Soddy (1913) termed isotopes. It was not until the discovery of the charge neutral neutron by Chadwick (1932) that it was recognized that isotopes were the consequence of the number of neutrons in the nucleus. Isotope geochemistry then grew from the recognition that the vast majority of elements have more than one isotope (e.g. Nier 1937) and that the abundances could be affected by geological processes.

In a seminal paper, Urey (1947) estimated the temperature-dependent fractionation of oxygen isotopes between $CaCO_3$ and water and proposed that this fractionation could be used as a geothermometer. Subsequently Epstein et al. (1953) calibrated the geothermometer by growing molluscs at different temperatures, initiating the field of stable isotope geochemistry.

One of the first stable isotope studies on ore deposits was by Engel et al. (1958a) on changes in the carbon and oxygen isotope composition of limestone in the Leadville district (Colorado, USA) due to hydrothermal alteration. This initiated a blossoming of stable isotope research on mineral deposits, and by the late 1960s and 1970s, stable isotope geochemistry, particularly the use of hydrogen, boron, oxygen, carbon and sulfur isotopes, had become one of the mainstays of ore genesis research, providing methods by which temperatures of mineral deposition could be estimated, sources of ore fluids, sulfur and some metals could be identified, and chemical reactions in ore forming systems could be tracked. Furthermore, as discussed by Barker et al. (2013) and others, stable isotopes have great potential as exploration vectors to many types of mineral deposits. As an example, variations in whole rock oxygen isotope values were one of the vectors that led to the discovery of the 45 West volcanic-hosted massive sulfide deposit in Queensland, Australia (Miller et al. 2001).

Contributions in this section illustrate how light stable isotopes have been used in the study

of and exploration volcanic-hosted massive sulfide (Huston et al. 2023), sediment-hosted base metal (Williams 2023), iron ore (Hagemann et al. 2023), and orogenic gold (Quesnel et al. 2023) systems. The use of stable isotopes in ore studies has been reviewed extensively, including in the second and third editions of *Geochemistry of Hydrothermal Ore Deposits* (Barnes 1979, 1997; Taylor 1979, 1997; Ohmoto and Rye 1979; Ohmoto and Goldhaber 1997). Other important overall reviews include those by Ohmoto (1986), Kerrich (1987), Taylor (1987), Seal (2006), and Shanks (2014), and there have been many reviews for specific deposit types. In addition, a number of more general reviews of stable isotope geochemistry have been published, including Valley et al. (1986), Kyser (1987), Valley and Cole (2001) and Hoefs (1997, 2021). This chapter provides context for the more detailed discussions of stable isotope geochemistry provided for individual mineral systems in later chapters.

2 Fundamentals of Light Stable Isotope Geochemistry

Light stable isotope geochemistry is concerned with variations in the relative abundance of stable isotopes of light elements, including hydrogen, helium, boron, carbon, oxygen, nitrogen, silicon, sulfur and chlorine. These elements share a number of characteristics: (1) low mass number, (2) large relative mass differences (difference in isotope mass relative to mass number) between the minor (generally the heavier) and the abundant isotope, and (3) sufficient abundance (>0.01%) of the minor isotope to allow precise measurements of the isotope ratio (Table 1). Of the above elements, only five—hydrogen, boron, carbon, oxygen and sulfur—are now used routinely in studies of mineral deposits and this review will concentrate on these elements. Helium (Simmons et al. 1987), nitrogen (Jia and Kerrich 1999), silicon (Zhou et al. 2007) and chlorine (Eastoe and Guilbert 1992) have also been used in mineral deposit studies, but not extensively, and are not discussed further.

3 Conventions, Definitions and Standards

Since the inception of stable isotope geochemistry as a separate field of geochemistry in the middle part of the last century, a set of conventions have been developed so that isotope data are reported systematically throughout the world. These conventions include definitions of notations used to report isotope data and standards to which isotope data are related.

The absolute isotope ratio, R, which is defined as the ratio of the number of atoms of the heavy isotope to that of the light isotope, is the fundamental parameter measured. However, differences in absolute ratios between two samples can be measured more precisely than absolute ratios. Consequently, the δ-value was introduced, which is a measure of the difference in absolute isotope ratios between the measured sample and a standard, to report the relative deviation of stable isotope abundances:

$$\delta_X(\permil) = 1000(R_X - R_{STD})/R_{STD}$$
$$= 1000(R_X/R_{STD} - 1) \qquad (1)$$

where R_X is the isotope ratio of an unknown sample and R_{STD} is the isotope ratio of a standard (McKinney et al. 1950). Because of the magnitude of most stable isotope variations in terrestrial materials, it is convenient to report the δ-value in per mil (‰) (Coplen 2011).

To facilitate interlaboratory comparisons, a set of international standards has been established for all geologically important light stable isotopes (Coplen et al. 1983). For hydrogen and oxygen, the internationally accepted reference standard is V-SMOW (Vienna[1] Standard Mean Oceanic Water; identical to the original SMOW); for boron the reference standard is NIST 951 (boric acid); for carbon the accepted reference standard is V-PDB (Vienna Peedee Belemnite; V-PDB is used as a reference standard for oxygen in some studies); and for sulfur the reference standard is V-CDT (Vienna Canyon Diablo

---

[1] Vienna denotes standard defined by the International Atomic Energy Agency based in Vienna.

Table 1 Characteristics of light stable isotope systems commonly used in mineral system studies and mineral exploration

Isotope system	Abundances of stable isotopes[1]	Isotope ratios of international standards
Hydrogen	[1]H: 99.9885% [2]H (D or deuterium): 0.0115% [3]H (tritium) is a man-made radioactive isotope that does not naturally exist	V-SMOW[2] $^{2}H/^{1}H$: 155.75 ($\pm$0.08) $\times 10^{-6}$
Boron	[10]B: 19.9% [11]B: 80.1%	NIST 951[3] $^{11}B/^{10}B$: 4.04362 ($\pm$0.00137)
Carbon	[12]C: 98.93% [13]C: 1.07% [14]C is a radioactive isotope with a short half-life that is produced by the interaction of cosmic rays with [14]N	V-PDB[4] $^{13}C/^{12}C$: 11,180.2 ($\pm$2.8) $\times 10^{-6}$
Oxygen	[16]O: 99.757% [17]O: 0.038% [18]O: 0.205%	V-SMOW[2] $^{18}O/^{16}O$: 2005.20 ($\pm$0.45) $\times 10^{-6}$ $^{17}O/^{16}O$: 379.9 ($\pm$0.8) $\times 10^{-6}$ V-PDB[4] $^{18}O/^{16}O$: 2067.2 $\times 10^{-6}$ $^{17}O/^{16}O$: 386.0 $\times 10^{-6}$
Sulfur	[32]S: 94.93% [33]S: 0.76% [34]S: 4.29% [36]S: 0.02%	V-CDT[5] $^{34}S/^{32}S$: 44,150.9 ($\pm$11.7) $\times 10^{-6}$ $^{33}S/^{32}S$: 7877.29 $\times 10^{-6}$

Data sources: [1]Rosman and Taylor (1999), [2,4]Werner and Brand (2001), [3]Catanzaro et al. (1970) and [5]Ding et al. (2001)

Troilite). Table 1 gives the absolute abundance ratios (on an atomic basis) for these reference standards. Positive δ values imply that the heavy isotope (e.g. D (^{2}H), [11]B, ^{13}C, [18]O or [34]S) is enriched in the sample relative to the reference standard.

3.1 Isotope Systems

Table 1 summarizes the characteristics of the five major light stable isotope systems used in mineral systems research and exploration. Most of these systems (H, B and C) are characterized by two stable isotopes, but the oxygen and sulfur systems contain three and four isotopes, respectively. In addition, the hydrogen and carbon systems contain radiogenic isotopes that are produced by man-made nuclear reactions (^{3}H or tritium and [14]C: Health Physics Society 2011) or naturally by interaction of cosmic rays with the upper atmosphere (^{14}C and [3]H: Korff and Danforth 1939; Health Physics Society 2011). These radiogenic isotopes are generally not used for ore

genesis studies, but have utility in the study of young geological and archeological systems.

4 Fractionation of Stable Isotopes

Like other chemical components, isotopes can be involved in chemical reactions that change their abundances between two or more chemical substances. As an example, galena and sphalerite exchange sulfur isotopes according to the following reaction:

$$Zn^{34}S + Pb^{32}S = Zn^{32}S + Pb^{34}S \quad (2)$$
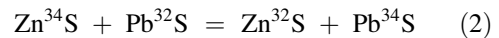
Like other chemical reactions, the equilibrium constant (K) can be expressed as follows:

$$
\begin{aligned}
K &= \alpha = (a_{Zn^{32}S}a_{Pb^{34}S})/(a_{Zn^{34}S}a_{Pb^{34}S}) \\
&= (a_{Pb^{34}S}/a_{Pb^{32}S})/(a_{Zn^{34}S}/a_{Zn^{32}S})
\end{aligned} \quad (3)
$$

where K and α are temperature dependent, and a_N indicates chemical activity of substance N. Because isotopes behave nearly ideally, the

above activity ratios are essentially identical to isotope ratios, and the above equation reduces to the isotope fractionation α:

$$\alpha = R_{PbS}/R_{ZnS} \qquad (4)$$

The difference in isotope composition between two minerals is commonly expressed as Δ_{A-B}, which is defined as $\delta_A - \delta_B$. Using the approximation that $1000\ln X \approx X$ (valid only if $X \sim 1.00$) and the definitions of R and δ, α_{A-B} is related to Δ_{A-B} as follows:

$$1000\ln\alpha_{A-B} \approx \Delta_{A-B} \qquad (5)$$

For Δ_{A-B} less than 10‰, this approximation is correct to within 0.25‰. For $|\Delta_{A-B}|$ greater than 10‰, the approximation becomes less accurate and isotope fractionation should be determined using the exact relationship between α and δ:

$$\begin{aligned}\alpha_{A-B} &= (1 + \delta_A/1000)/(1 + \delta_B/1000) \\ &= (1000 + \delta_A)/(1000 + \delta_B)\end{aligned} \qquad (6)$$

For isotope systems in which fractionation is relatively small (e.g. oxygen and boron), the approximation is mostly valid, for but for the hydrogen, carbon and sulfur systems, in which fractionations can reach 100‰, the exact relationship should be used.

The fractionation of isotopes has been studied experimentally and theoretically for many minerals (c.f. Taylor 1979; Ohmoto and Rye 1979; Kieffer 1982; Clayton and Kieffer 1991; Kowalski and Wunder 2018, and many others). These data form the basis from which isotope data can be interpreted in a geologically meaningful manner. Readers are referred to Beaudoin and Therrien (2009) and the related web-based and macOS/iOS/padOS/Android AlphDelta isotope calculator (http://alphadelta.ggl.ulaval.ca) for an up-to-date compilation of these data for hydrogen, carbon, oxygen and sulfur and a tool for fractionation and equilibrium temperature isotope calculations.

4.1 Multiple Isotope Measurements

This convention so far considers mass-dependent fractionation, which can be expressed from the ratio of two isotopes of an element. This is sufficient for analysis and consideration of δD, $\delta^{11}B$, $\delta^{13}C$, and $\delta^{18}O$. While oxygen has another minor isotope ^{17}O, and its abundance is important in atmospheric chemistry, its use for ore studies has just begun (Peters et al. 2020), and multiple oxygen isotope analysis is not considered further here. However, for sulfur isotopes the abundances of the other minor isotopes are increasingly being used to examine potential processes affecting sulfide formation (one of the earliest examples of this is the study of Hulston and Thode 1965), and so some consideration of multiple isotope measurements is required.

Sulfur has four stable isotopes ^{32}S, ^{33}S, ^{34}S, and ^{36}S. As described above, the two-isotope ratio $^{34}S/^{32}S$, and hence $\delta^{34}S$, is generally used to consider an isotope fractionation related to mass dependent fractionation. Based on $\delta^{34}S$, a prediction can therefore be made concerning the magnitude of $\delta^{33}S$ and $\delta^{36}S$ in any sample. This can be considered in terms of relative mass difference from the major isotope. If the isotope fractionation is 1.0‰ for $\delta^{34}S$, then the prediction will be that $\delta^{33}S$ will be about 0.5‰ [0.5 being obtained from (33–32)/(34–32)], and $\delta^{36}S$ will be about 2.0‰ [2 being (36–32)/(34–32)]. This approximation can be refined using exact nuclidic masses, and also by changing the mass fractionation law that relates $\delta^{33}S$ and $\delta^{36}S$ to $\delta^{34}S$ (e.g. linear, power, exponential).

Another isotope parameter (Δ) can then be determined for the difference in isotope abundance measured, versus that predicted based on $\delta^{34}S$. A common formalism for $\Delta^{33}S$ and $\Delta^{36}S$ can be expressed as[2]:

$$\Delta^{33}S = \delta^{33}S_X - 0.515\delta^{34}S_X \qquad (7)$$

and

---

[2] These definitions of $\Delta^{33}S$ and $\Delta^{36}S$ differ from that of $\Delta^{34}S$, which indicates the difference in isotopic composition between two minerals, that is $\Delta^{34}S_{A-B} = \delta^{34}S_A - \delta^{34}S_B$.

$$\Delta^{36}S = \delta^{36}S_X - 1.90\delta^{36}S_X \qquad (8)$$

where the values 0.515 and 1.90 represent the mass differences based on the exact nuclidic masses, and a linear mass-dependent relationship is assumed. For mass dependent fractionation, $\Delta^{33}S$ and $\Delta^{36}S$ will be 0 ‰; for non-mass-dependent fractionation, or, mass independent fractionation, $\Delta^{33}S$ and $\Delta^{33}S$ can be non-zero. It should be noted that the normalized abundances of $\Delta^{33}S$ and $\Delta^{36}S$ are based on the concurrent measurements of $\Delta^{34}S$, with $\Delta^{33}S$ and $\Delta^{36}S$ and so the precision of $\Delta^{33}S$ and $\Delta^{36}S$ is not a function of the external reproducibility of $\Delta^{34}S$ in a sample suite.

5 Analytical Methods

Since the first description of analytical techniques for carbon and oxygen isotope analyses of carbonate minerals by McCrea (1950), analytical methods have evolved to the point where for most stable isotope systems, procedures exist that allow the analysis of less than a few pictograms (pg: 10^{-12} g) of sample for micro-analytical methods. As the methods for stable isotope analysis is a wide field and a number of volumes have reviewed the analytical techniques (e.g. de Groot 2004, 2009; Foster et al. 2018), the description below is brief.

In a broad sense, analytical methods for stable isotopes can be grouped into bulk methods that generally produce a gas that is analysed by a gas-source isotope ratio mass spectrometer, and microanalytical methods that generally extract material from the sample using either a laser or an ion beam followed by analysis using gas-sourced mass spectrometry, inductively coupled plasma mass spectrometry (ICP-MS) or secondary ion mass spectrometry (SIMS). Bulk methods, which were developed in the 1950s and 1960s, are still the mainstay for analyses in many laboratories. In contrast, microanalytical methods began to be developed in the 1980s and 1990s, and are only now becoming widespread as the number of instruments has increased and the relative costs of analyses have decreased.

5.1 Bulk Analytical Methods

Most bulk stable isotope analytical methods involve the conversion of solid minerals into gases that can be analysed using gas-source mass spectrometry. Carbonate minerals are typically reacted with phosphoric acid at various temperatures (depending on the mineral) to produce CO_2, which is then analysed for $\delta^{13}C$ and $\delta^{18}O$ (McCrea 1950). Typical external uncertainties (2σ)[3] for this method are 0.10‰ for $\delta^{13}C$ and 0.16‰ for $\delta^{18}O$.

Sulfide minerals are typically reacted with excess CuO at 800–1000 °C, with the sulfide converted to SO_2 gas, which is analysed for $\delta^{34}S$ (Grinenko 1962; Robinson and Kusakabe 1975). Alternatively, sulfide minerals can be reacted with BrF_5 or ClF_3 to produce SF_6 gas, which is then analysed (Puchelt et al. 1971). This latter method has an important advantage over the SO_2 method in that fluorine has only one isotope (versus three for oxygen), removing uncertainties in analysis due to non-S isotope variations. As a consequence, the fluorination method is used in multiple sulfur isotope studies (Rumble et al. 1993). External uncertainties (2σ) for the SO_2 method are typically 0.2–0.3‰ for $\delta^{34}S$, and uncertainties for the SF_6 method are typically 0.2‰. For $\Delta^{33}S$ and $\Delta^{36}S$, uncertainties of the order of 0.04 ‰ and 0.4 ‰ (2σ) reflect the relative abundances of ^{33}S and ^{36}S (Farquhar et al. 2007).

As the reagents that have traditionally been used to fluorinate sulfide (and other) minerals (BrF_5, ClF_3 and F_2) are hazardous and difficult to handle, Ueno et al. (2015) developed a rapid technique for fluorination of Ag_2S using solid CoF_3 as the fluorination agent. Following reaction at 590 °C using a Curie-point pyrolyzer, the resulting SF_6 gas was purified using a combination of cryogenic cleaning and gas

---

[3] To be consistent with radiogenic isotope systems, uncertainties cited here are external 2σ values. `External' refers to uncertainties determined from repeat analyses of individual samples or standards; internal uncertainties, which are usually less than external uncertainties, refer to uncertainties due to counting statistics on individual analyses.

chromoatogarphy. Details are provided by Ueno et al. (2015) and Caruso et al. (2022). External (2σ) uncertainties are 0.7‰ for $\delta^{34}S$, 0.01‰ for $\Delta^{33}S$ and 0.2‰ for $\Delta^{36}S$.

Prior to analysis, sulfate minerals are typically converted to Ag_2S using two methods. In the first method, described by Rafter (1957), the sulfate minerals are first dissolved, then precipitated as barite after the addition of $BaCl_2$ to the solution. The barite is reduced with graphite at 900–1050 °C to produce BaS and CO_2, then the BaS is dissolved and AgCl added to precipitated Ag_2S. Alternatively, the sulfate minerals are boiled either in an $HI-H_3PO_2-HCl$ solution (Thode et al. 1961) or in Kiba reagent (Sasaki et al. 1979) to convert sulfur into H_2S, which is then precipitated as Ag_2S with the addition of AgCl. The Ag_2S produced in both methods is analysed using either the CuO reaction or fluorination methods described above for sulfide analysis. The graphite-reduction method has the advantage that $\delta^{18}O$ can also be determined from the CO_2 produced.

Oxygen is extracted from rocks and minerals by fluorination of the rock with either BrF_5 or ClF_3 at temperatures of 450–690 °C, depending on the mineral being analysed. The heating is done either with a heating element surrounding the reaction vessels or with lasers. This produces O_2 gas, which, historically, has been converted to CO_2 gas by Pt-calatysed reaction with graphite (Clayton and Mayeda 1963), although many laboratories currently use O_2 directly. The CO_2 or O_2 gas is then analysed. This method typically produces external uncertainties (2σ) in $\delta^{18}O$ of 0.2–0.4‰.

Hydrogen isotope analysis of whole rocks, minerals and fluid inclusions involves a fairly complicated procedure to produce H_2 gas suitable for mass spectrometry. First the sample is heated to 150–200 °C under vacuum for several hours to remove adsorbed water. After the adsorbed water has been removed, whole rock and mineral samples are heated to a temperature of 900 °C using either a resistance furnace or an induction oven to release water, which is collected on a liquid N_2 trap. To analyse fluid inclusions, after removal of adsorbed water, (generally) quartz chips are heated to 800 °C, which decrepitates the fluid inclusions, and water and other gases are collected using liquid N_2. After cryogenic purification, the collected water is then reduced to form H_2 gas using either heated uranium (Bigeleisen et al. 1952) or zinc (Vennemann and O'Neil 1993), with the H_2 gas then being analysed. This method typically produces external uncertainties (2σ) in δD of 4‰. It must be stressed that fluid inclusion decrepitation results in the collection of the mixing of all types of inclusions, which can introduce significant uncertainties in interpreting the resulting data.

Production of gases for bulk isotope analyses is always conducted on vacuum lines with all conversions *in vacuo*, and the resulting gases cleaned of impurities cryogenically. In most methods gas conversion is undertaken at high temperatures and involves the use of furnaces. In addition, preparation of SF_6 and O_2 by fluorination involves strong, and dangerous, oxidants. Hence, preparation of all gases for gas-sourced mass spectrometry has a degree of hazard, which some (though not all) micro-analytical methods eliminate.

In addition to the preparation methods described above, many laboratories use elemental analyzers to combust solids and produce gases such as CO_2 and SO_2, which are separated automatically using gas chromatography and analyzed by gas-source mass spectrometry (Pichlmayer and Blochberger 1988; Giesemann et al. 1994). With the removal of the need for cryogenic cleaning of the analyzed gases, this development has simplified analytical methods and made them much more rapid.

Bulk analytical methods for boron isotopes differ from those used for other light stable isotopes in that analysis is undertaken using either thermal ionization mass spectrometry (TIMS) or inductively-coupled plasma mass spectrometry (ICP-MS) rather than gas-source mass spectrometry. As a consequence, preparation for analysis involves solution chemistry and purification, whereby care is needed to avoid partial loss of volatile boron and resulting isotope fractionation. Details of sample preparation are described in detail by Sah and Brown (1997), Aggerwal and

You (2016) and Foster et al. (2018). Historically, boron isotopes were generally analysed using TIMS, but the development of ICP-MS analysis in the late 1990s has enabled much easier and more rapid analysis. TIMS analyses are done using positive (PTIMS) or negative ions (NTIMS), the pros and cons of which are described in the specialized literature cited. TIMS analysis yields a typical uncertainty (2σ) of 0.4–0.6‰, whereas ICP-MS analysis has an (2σ) uncertainty of 0.2–0.3‰ (c.f. Foster et al. 2013).

5.2 Micro-analytical Methods

The development of micro-analytical tools for analyzing stable isotopes began in the late 1980s and continues today, with both the spatial resolution and precision of the analyses improving. Micro-analytical methods have used two different techniques to extract and analyse samples: laser ablation followed by gas-source isotope ratio mass spectrometry or inductively-coupled-plasma mass spectrometry (ICP-MS, including triple quadrapole ICP-MS—ICP-QQQ-MS), and secondary-ion mass spectrometry (SIMS) utilising a focused ion beam of oxygen or cesium. The two techniques have both advantages and disadvantages. Laser-based systems tend to provide faster and less expensive analyses, but the analyses can have lower spatial and analytical precision and are relatively destructive. In contrast, secondary-ion mass spectrometry is slower and more expensive, but it can have better spatial and analytical precision, greater sensitivity, and is much less destructive, which can be important if multiple analyses are to be carried out of the same points.

5.2.1 Laser Heating and Laser Ablation

Lasers can be used in two distinct ways for isotope analysis – either for heating a small and localized sample, or for direct ablation. Isotope analysis by laser heating gas source isotope ratio mass spectrometry involves laser heating of a sample with an oxidant (O_2, or F_2) in a reaction chamber prior to purification of the product gas (O_2, SO_2 or SF_6: Elsenheimer and Valley 1992;

Sharp 1990; Beaudoin and Taylor 1994) using cryogenic or chromatographic techniques, and measurement of the stable isotope composition by gas-source mass spectrometry. The advantage of the laser for heating is that localized heating of the sample can be effected without involving the container (crucible); hence blanks can be limited allowing smaller samples to be analysed. One of the first uses of laser heating for microanalysis was to determine $\delta^{18}O$ and $\delta^{34}S$ from silicate and sulfide minerals. Small crystals or small aliquots of powders are laser-heated using typically a Nd:YAG or CO_2 laser in a F_2 or BrF_5 (or ClF_3) atmosphere for oxygen analysis, or additionally with an O_2 atmosphere for sulfur analysis (Crowe et al. 1990; Kelley and Fallick 1990; Sharp 1990; Elsenheimer and Valley 1992; Akagi et al. 1993; Beaudoin and Taylor 1994).

Laser ablation, which can occur in both reactive and inert atmospheres, typically produces a crater 50–200 μm in diameter, depending on the mineral being ablated and laser power and focus. The depth of the pit is typically of a similar dimension. Reaction of the ablated mineral with a reactive atmosphere produces SO_2 (sulfide mineral in O_2 atmosphere), SF_6 (sulfide mineral in F_2, BrF_5 atmosphere) or O_2 (silicate or oxide mineral in BrF_5 atmosphere). In some systems the product gas is then cleaned offline and, in the case of oxygen, converted into CO_2 before analysis. In other systems, the product gas is automatically cleaned cryogenically or by gas chromatography and then directly introduced into the mass spectrometer for analysis. Laser ablation and a reactive atmosphere produces a reproducible, but mineral- and laboratory-dependent, fractionation effect that has to be corrected to produce final results. The typical external (2σ) errors associated with laser ablation are typically 0.2–0.4‰ for $\delta^{34}S$ and 0.2–0.6‰ for $\delta^{18}O$.

Laser ablation in an inert atmosphere has supplanted that in a reactive atmosphere. In this method ablation products are introduced directly into a (multi-collector) inductively coupled plasma mass spectrometer with a carrier gas (commonly He and/or Ar) (Mason et al. 2006; Bendall et al. 2006). These methods typically produce external errors (2σ) of 0.3–0.6‰.

Boron analysis using laser-ablation ICPMS has advantages of greater speed than SIMS and more flexibility in that it places lower demands on surface quality and is less strictly dependent on matrix-matched reference materials (but see Mikova et al., 2014). Studies report a similar level of external uncertainty as for SIMS (1‰ at 2σ). The main disadvantage, however, is the larger spot size and deeper penetration depth of the laser compared to the ion beam. In many cases a larger spot size is required as a greater volume of material is required for analysis if the boron concentrations are low.

5.2.2 Secondary Ion Mass Spectrometry

SIMS uses a focused ion beam, e.g. O^- or Cs^+, to ablate the sample. The interaction of the primary ion beam (10–20 keV) with the target leads to secondary ionization. The probability of ionization is element specific, with metals producing positive secondary ions with O^- primary ion beam, and non-metals being ionized to negative secondary ions with a Cs^+ ion beam. The chemistry of the ion beam also aids in ionization with electronegative oxygen producing strong electropositive element secondary ion beams and electropositive cesium producing strong electronegative element secondary ion beams (Ireland 1995). As such, SIMS differs from LA in that an ion beam is produced directly from the target. This makes it a sensitive technique, but also strongly matrix dependent and so mineral standards of close composition to the target minerals are required.

SIMS was initially developed in geochemistry in an attempt to measure trace element abundances that were inaccessible by electron beam techniques in the 1960s. The capability to examine radiogenic isotope systems was not developed until the SHRIMP ion microprobes when the combined issues of transmission (sensitivity) and high mass resolution were addressed. While stable isotope analysis does not require high sensitivity or high mass resolution, the low transmission of early instruments led to variable measured isotope compositions simply because of differences in ion paths through the

instruments (Shimizu and Hart 1982). SIMS has also been applied to measuring stable isotopes including those of hydrogen, boron, carbon, oxygen, and sulfur. As such, early analyses suffered from reproducibility at a level of greater than one permil for oxygen and sulfur isotope systems (Valley and Graham 1991; Eldridge et al. 1987). Subsequent developments have led to much higher reproducibility with external uncertainties (2σ) of 0.3‰ for $\delta^{18}O$ analyses (e.g. Kita et al. 2009) and 0.3‰ for $\delta^{34}S$ analyses (e.g. Paterson et al. 1997; Kita et al. 2010). Moreover, recent developments have allowed analysis of all isotope ratios in both the oxygen (e.g. $\delta^{17}O$ and $\delta^{18}O$) and sulfur ($\delta^{34}S$, $\delta^{33}S$ and $\delta^{36}S$) isotope systems with similar uncertainties (Ireland et al. 2014).

A key aspect in stable isotope analysis is the development of multiple collection whereby all isotopes are measured at the same time thereby cancelling the uncertainty associated with the primary ion beam noise. This is now the standard methodology for large sector ion microprobes. For $\delta^{18}O$ measurements, sufficient $^{18}O^-$ is produced for analysis of both $^{18}O^-$ and $^{16}O^-$ in Faraday cup multiple collection mode. Similarly, for sulfur, ^{32}S, ^{33}S, and ^{34}S can be measured by Faraday cups. However, the low abundance ^{36}S cannot be measured with the Faraday cups using high-ohmic resistors because of the Johnson noise associated with the circuitry. Measurements of ^{36}S can use either an ion counter, or Faraday cup electrometers using charge mode (accumulation of charge across a capacitor). Precision for in situ analysis of $\Delta^{33}S$ can be better than 0.1 ‰ while $\Delta^{36}S$ measurements by electron multiplier are around 1 ‰ (2σ) (Whitehouse 2013) and around 0.4 ‰ (2σ) by charge mode (Ireland et al. 2014).

While the large sector ion microprobes are used to pursue highest precision stable isotope analyses, the nanoscale-SIMS offers high spatial resolution analysis. A typical "spot" for high precision stable isotope analysis is typically 10–30 µm, which allows sufficient material to be sampled to give sufficient ions for the required counting precisions. However, the purpose of the nanoscale-SIMS is to analyse targets at the

100 nm scale. At this sampling scale, only major isotopes can be measured to high precision.

Boron analysis by magnet-sector SIMS is commonly done with instruments set for mono-collection and mass-switching between [11] and [10]B, but multi-collection SIMS is routinely used in some installations of the large-geometry instruments. The external uncertainty obtained by mono-collection SIMS is typically between 1 and 2‰ (2σ), whereas multi-collection of the two isotopes can reduce this uncertainty by about half. Those values refer to "high-concentration" samples like tourmaline, which can contain percent levels of B. For low-concentration samples, often with less than 20 ppm B, the analytical precision may be limited by counting statistics. For example, large-geometry SIMS instruments have achieved precision of about 3‰ for samples with 1 ppm B (Foster et al. 2018).

An important, and for some applications limiting, issue for all SIMS analysis is the need for matrix-matched reference materials that are homogeneous on the micron scale or better. Such are available and internationally distributed for only a limited number of geologically relevant materials for stable isotope analysis. These include glass, tourmaline, carbonates, silicates/oxides and sulfides; these are primarily standards for mass-dependent fractionation. Further development is required for minor isotope abundances (e.g. for $\Delta^{33}S$ and $\Delta^{36}S$), boron isotope measurements at low levels, as well as a wider range of minerals relevant to ore deposits.

6 Processes That Fractionate Light Stable Isotopes

Fundamentally, fractionation of light stable isotopes is the result of small differences in translational, rotational and vibrational motions of bonds within the respective phases. Although it is beyond the scope of this review (see Kieffer 1982 for more details), bonds involving heavier isotopes are marginally stronger than bonds involving lighter isotopes of the same element. This effect is strongly dependent upon the relative mass difference ($RMD = (AM_H - AM_L)/AM_L$, where

AM_H = atomic mass of heavy isotope and AM_L = atomic mass of light isotope) between isotope pairs: the effect is much stronger between hydrogen (^1H) and deuterium (^2H) (RMD $\sim$ ((2–1)/1) = 1) than between isotopes of heavier isotopes (e.g. ^{34}S and ^{32}S; RMD $\sim$ (34–32)/32 = 0.0625). Hence, isotope fractionation in the hydrogen system is much greater than that in the boron, carbon, oxygen and sulfur systems, in the absence of kinematic and biologic processes (C, S), and fractionations in light isotope systems are greater than fractionations in stable metal systems (e.g. Fe, Cu and Zn: Lobato et al. 2023; Mathur and Zhao 2023; Wilkinson 2023).

All geochemical processes involve some isotope fractionation, although for heavy elements (e.g. Pb, U), this effect is generally not measurable. The amount of fractionation depends not only on relative mass differences, but also on the type of geochemical reaction and the temperature at which the reaction occurs. For most stable isotope systems, the magnitude of isotope fractionation decreases with increasing temperature (Fig. 1), with mass dependent fractionation functions (except hydrogen) generally having the form:

$$1000\ln\alpha_{A-B}(\Delta_{A-B}) = A/T^2 \times 10^6 + B/T \times 10^3 + C$$

(9)

where T is temperature in Kelvin and A, B and C are experimentally- or theoretically-determined constants. This temperature dependence of isotope fractionation between minerals can be used to estimate paleotemperatures of mineral deposition (see below).

Most geochemical reactions can be divided into two general groups: those reactions that do not involve electron exchange, and those that do (redox reactions). In general, redox reactions involve much larger isotope fractionations. For example, $\Delta^{34}S$ at 300 °C for the reaction between sphalerite and aqueous H_2S, which is not a redox reaction, is 1.5‰, whereas $\Delta^{34}S$ at 300 °C for the reaction between anhydrite and aqueous H_2S, which is a redox reaction, is 22.0‰ (calculated using Alpha-Delta (Beaudoin
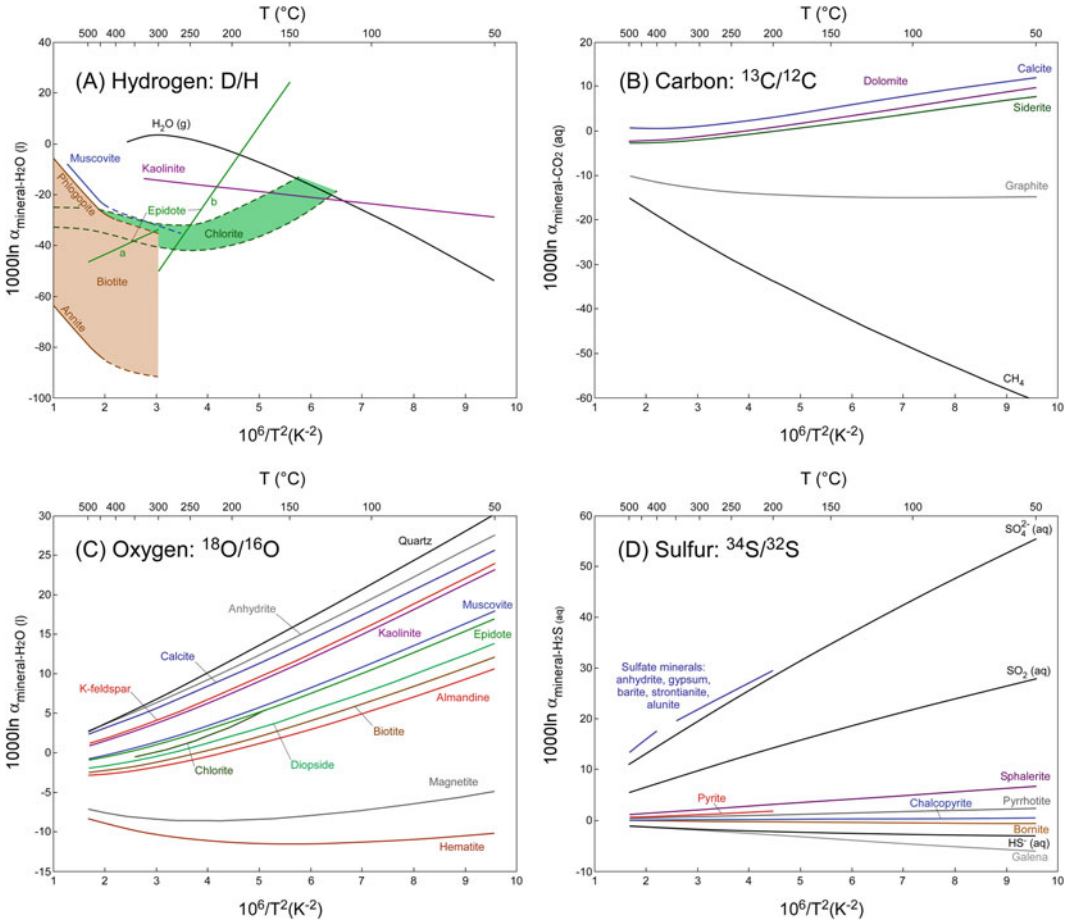
Fig. 1 Temperature versus 1000 ln α diagrams for the (A) hydrogen (1000 ln $\alpha_{mineral\text{-}H2O\ (l)}$), (B) carbon (1000 ln $\alpha_{mineral\text{-}CO2\ (aq)}$), (C) oxygen (1000 ln $\alpha_{mineral\text{-}H2O\ (l)}$) and (D) sulfur (1000 ln $\alpha_{mineral\text{-}H2S\ (aq)}$) isotope systems. For some systems, fractionation curves are also shown for dissolved species. Updated from Taylor (1979) and Ohmoto and Rye (1979). For hydrogen, isotope data of Taylor (1979: biotite and muscovite), Chacko et al. (1999: epidote curve a (300–600 °C)), Graham et al. (1980: epidote curve b (150–300 °C)), Gilg and Sheppard (1996: kaolinite) and Horita and Wesolowski (1994: H$_2$O vapor) were used. For carbon, isotope data of Ohmoto and Rye (1979) were used. For oxygen, isotope data of Cole and Ripley (1998: chlorite), Sharp et al. (2016: quartz), Zheng (1993a: almandine, diopside and K-feldspar), Zheng (1993b: biotite, epidote, kaolinite and muscovite), Zheng (1999: anhydrite and calcite), and Zheng and Simon (1991: hematite and magnetite) were used. For sulfur, isotope data of Eldridge et al. (2016: SO$_2$ (aq) and SO$_4^{2-}$ (aq)), Li and Liu (2006: bornite, chalcopyrite, galena, pyrrhotite andsphalerite), and Ohmoto and Rye (1979: sulfate minerals (anhydrite, gypsum, barite, strontianite and alunite) and pyrite), were used

and Therrien 2009); most fractionation factors discussed below are calculated similarly). Moreover, redox reactions include some reactions, such as disproportionation, and photolytic and biogenic reactions, that are characterized by distinctive isotope effects, and at low temperatures (<250–300 °C), kinetic effects can strongly effect isotope fractionation.

6.1 Reactions Not Involving Reduction or Oxidation

Reactions that do not involve electron exchange are many and varied, but the most important reactions in mineral systems (and geological systems in general) involve the transition between liquid and solid. In some systems (e.g.

involving H and O) the transition between liquid and gas is also important.

The simplest reactions involve a physical phase change without a compositional change. Examples include boiling of pure water, condensation of steam or the recrystallization of aragonite to form calcite. Although these reactions involve changes in physical parameters such as density, the chemical composition of the reactants and products do not change. However, the isotope composition does change: $\Delta^{18}O_{liquid-vapour}$ for boiling or evaporation of pure H_2O is 2.5‰ at 200 °C.

Although phase changes are important for some mineralising processes (e.g. boiling in some epithermal systems), by far the most important processes in mineral systems involve dissolution or melting in, or precipitation of minerals from, aqueous fluids or magmas. Processes whereby ore metals and other components are extracted from source rocks into a transporting media generally involve either melting of rocks to form a metal-bearing magma or water–rock reaction to form a metal-bearing aqueous fluid. In contrast, processes whereby metal is extracted from the melts or hydrothermal fluids to form mineral deposits generally involve precipitation or crystallization of ore and gangue minerals from these fluids. Isotope data can be very useful in tracing these processes. A third type of chemical reaction involves changing the speciation and complexing of components within hydrothermal fluids. This type of reaction may not be observable in rock chemistry, but in some cases, it can result in isotope fractionation. The last group of processes involves the formation of two immiscible fluids from an original fluid. Examples include the exsolution of an immiscible sulfide melt from a parent silicate magma or the exsolution of an aqueous magmatic-hydrothermal fluid during crystallization of a silicate magma.

As the exsolution of a magmatic-hydrothermal fluid from a crystallising magma occurs at magmatic temperature (700–1000 °C: Burnham 1979), and oxygen isotope fractionation at these temperatures is small, the inferred oxygen isotope composition of the magmatic-hydrothermal fluid (5.5–10.0‰: Taylor 1979) overlaps with that of igneous rocks (5.5–11.0‰: Taylor and Sheppard 1986).

The reaction of hydrothermal fluids with rocks causes significant changes to the mineralogy and chemical and isotope composition of the rock and of the fluid, as a function of temperature and atomic water/rock ratios. This process of hydrothermal alteration is dominated by hydrolysis. Many alteration minerals (e.g. sericite, chlorite, epidote and others), which are enriched in H_2O or OH^- relative to the rock-forming minerals they have replaced, are the product of hydrolytic reactions in which water has been added to the rock. Tourmaline is a special case in this regard because it is not only a hydrous mineral but it is commonly the only mineral sink for boron in alteration assemblages. If the fluid/rock ratio is high (as is generally the case for pervasive alteration assemblages), the isotope composition of the altered rock is determined by that of the altering fluid. In these cases, the isotope composition of the altering fluid can be estimated from the isotope composition of the altered rock, and, in some cases, the source of this fluid can be inferred.

The last non-redox process that affects isotope characteristics in geological systems is mixing between components with differing isotope compositions that does not involve redox reaction. Mixing can result in significant gradients in isotope ratios, which can be used to identify and map this process (see below). This process commonly is an important mechanism of ore deposition, with important applications for mineral exploration.

6.2 Redox Reactions

Many elements involved in chemical reactions in geological systems exist in multiple valence states. In mineral systems the most important multivalent elements are Fe (Fe^0, Fe^{2+} and Fe^{3+}), S (S^{2-}, S^0, S^{4+} and S^{6+}) and C (C^{4-}, C^0, C^{4+}). Many of the reaction types discussed above can involve changes in valency and if so, they are considered redox reactions. An important

characteristic of most redox reactions is that while one element is reduced (i.e. gained electrons) during the reaction, another must be oxidized (i.e. lost electrons). Redox reactions generally involve strong isotope fractionation, because of the equilibrium between the reduced species forming lower bond energy compounds (e.g. H_2S, CH_4) with higher bond energy in oxidized compounds (e.g. SO_4, CO_2). Hence, large variations in isotope ratios can be an indicator of redox reactions, particularly those involving S, C and Fe (the importance of redox in Fe isotope fractionation is discussed by Lobato et al. 2023).

Figure 2a illustrates the variations in $\Delta^{34}S_{H2S\text{-}fluid}$ as a function of pH and f_{O2} (i.e. redox) at a temperature of 250 °C. Although current fractionation data indicate no significant gradients are present as a function of pH, there is a strong gradient in $\Delta^{34}S_{H2S\text{-}fluid}$ just below the boundary between the hematite and pyrite stability fields (c.f., Ohmoto 1972). This gradient reflects the relative abundance of reduced S (H_2S and HS^-) and oxidized S (H_2SO_4, HSO_4^- and SO_4^{2-}) species, which is a reflection of the oxidation state of the system (i.e. $\Sigma SO_4/\Sigma H_2S$, f_{O2} and f_{H2}). Hence, if a large gradient in $\delta^{34}S$ exists either in space or time (i.e. paragenesis), this gradient could indicate the presence of redox reactions involving S species, particularly if accompanied by changes in Fe-S–O mineralogy.

Ohmoto (1972) indicated that carbon isotopes can experience shifts as a consequence of redox reactions involving graphite and carbonate minerals. Figure 2b shows variations in $\Delta^{13}C_{H2CO3\text{-}fluid}$ as a function of f_{O2} and pH at 250 °C. There is a strong gradient in $\Delta^{13}C_{H2CO3\text{-}fluid}$ that corresponds to the conversion of the C^{4-} to C^{4+} in the lower part of the pyrite field. Hence gradients in $\delta^{13}C$ may indicate redox processes, although other geological processes (e.g. mixing) can also produce gradients.

Although Fig. 2 shows variations at 250 °C at specific conditions (details in caption), the
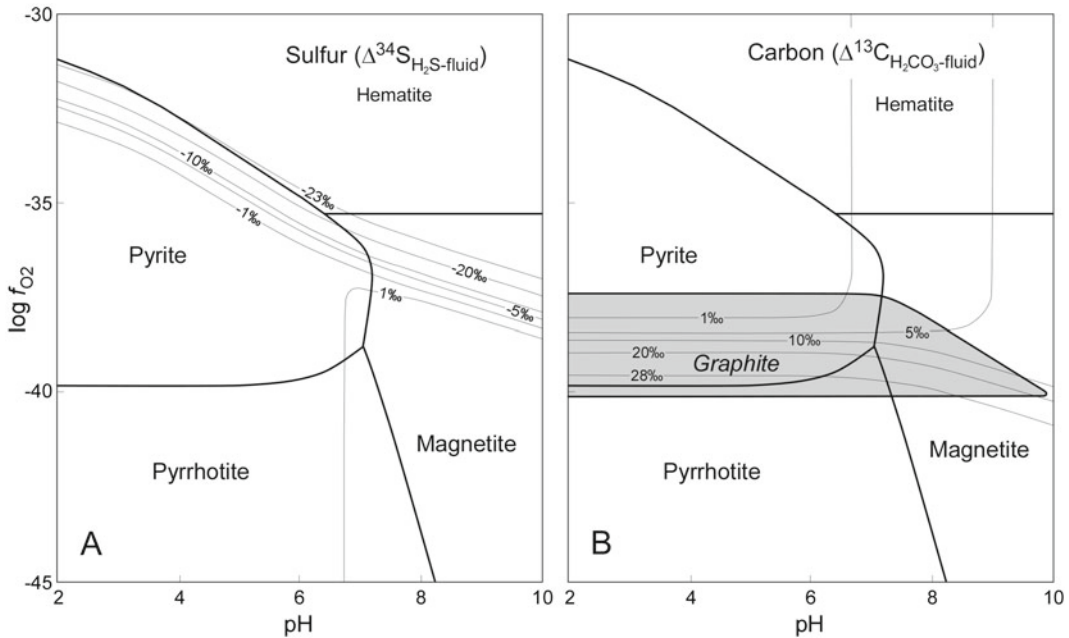

Fig. 2 Variations in (A) $\Delta^{34}S_{H2S\text{-}fluid}$ and (B) $\Delta^{13}C_{H2CO3\text{-}fluid}$ as a function of redox (f_{O2}) and pH at 250 °C. These diagrams are updated from the original diagrams in Ohmoto (1972) using updated thermodynamic and isotope fractionation data (Ohmoto and Rye 1979; Eldridge et al. 2016). The diagrams were calculated for a fluid with 5% dissolved NaCl, $10^{-2.5}$ m ΣS (~ 320 ppm S) and 1 m ΣC (~ 120 ppm C) taking into account activity coefficients and ion pairing

morphology of the diagram is retained for most hydrothermal conditions. For example, the gradient in $\Delta^{34}S_{H2S\text{-}fluid}$ near the upper margin of the pyrite field is retained at higher and lower temperature. Increasing the total sulfur content of the fluid expands the pyrite and, to a lesser extent, the pyrrhotite fields, but the sulfur isotope gradient is retained. Similarly, the gradient in $\Delta^{13}C_{H2CO3\text{-}fluid}$ also occurs near the bottom of the pyrite field and overlaps the graphite field under most hydrothermal temperatures.

Mixing of fluids with different redox characteristics can induce redox reactions and isotope fractionation. A good example of this is the mixing of relatively reduced H_2S-rich vapor generated by boiling of epithermal fluids into oxidized groundwater. As the gaseous H_2S is dissolved into groundwater, it is oxidized, producing sulfuric acid, which extensively alters rocks to aluminous assemblages (Simmons et al. 2005). In addition to the common hydrolytic, precipitation and mixing reactions, there are several special types of redox reactions that can have distinctive isotope effects, including disproportionation, photolytic and biologically-mediated reactions. In addition, many redox reactions are strongly affected by the speed, or kinetics, of reaction, which decreases as temperature decreases.

6.2.1 Disproportionation Reactions

Disproportionation reactions involve a reactant with intermediate valency producing products of higher valency and lower valency together. Unlike other redox reactions, disproportionation reactions do not necessarily involve valency changes to other chemical components during the reaction. The best example of such a reaction in mineral systems is the disproportionation of SO_2:

$$4SO_2 + 4H_2O \ = \ H_2S \ + \ 3H_2SO_4 \quad (10)$$
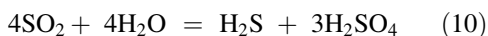
The most important role of SO_2 disproportionation in mineral systems is during the evolution of magmatic-hydrothermal fluids from moderately oxidized magmas. This reaction, which causes aluminous alteration due to the production of sulfuric acid, can produce distinctive isotope

effects: in many porphyry systems in which this process is important, $\Delta^{34}S_{sulfate\text{-}sulfide} \sim 5\text{–}20‰$ (mostly 7–18‰: Rye 2005; Seal 2006). Hence, isotope fractionation can be indicative that this (and other) processes have occurred in a mineral system.

6.2.2 Mass-Independent Fractionation and Photolytic SO_2 Dissociation

For most reactions involving elements with three or more isotopes, fractionation between isotopes is `mass-dependent', that is the fractionation between isotopes is dependent on relative mass differences. In most cases $\delta^{17}O = 0.525\text{–}0.528 \times \delta^{18}O$ (Young et al. 2002; Pack and Herwartz 2014; Sharp et al. 2016), and $\delta^{33}S = 0.515 \times \delta^{34}S$ (Fig. 3a; Hulston and Thode 1965; Johnston 2011). Clayton et al. (1973, 1977), however, found that for O isotope fractionation within carbonaceous chondritic meteorites, the mass-dependent relationship did not hold. Subsequent studies have established this for anhydrous minerals from carbonaceous chondrites as well, where $\delta^{17}O = 0.941 \times \delta^{18}O$ - 4.00 (Clayton 2003). Although it is beyond the scope of this contribution,[4] these meteoritic effects identified "mass-independent" isotope fractionation (MIF) for the first time (Ireland 2012). Subsequent studies found that the formation of ozone (Heidenreich and Thiemens 1986; Mauersberger 1987) and the photolytic dissociation of gaseous SO_2 (Farquhar et al. 2001) also involved MIF although it remains to be seen whether the MIF associated with ozone fractionation is related in any way to the ^{16}O variability in meteorites.

Photolytic dissociation of SO_2 and other S-bearing gases in the ancient (i.e. pre 2400 Ma) atmosphere was controlled by two factors, the abundance of the gas, and the shielding effects of other gas molecules (e.g. O_2 and O_3) present in the atmosphere (Farquhar et al. 2000; Lyons 2007; Ueno et al. 2009). The most important factor is likely shielding by O_2 and O_3, which

---

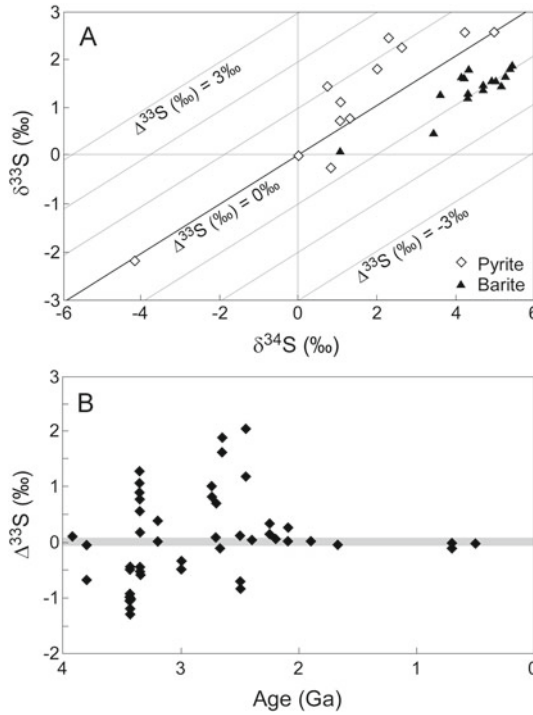[4] See Clayton 2003 for more details and processes that cause fractionation in meteorites.

Fig. 3 Diagrams (modified after Farquhar et al. 2000) showing mass-independent fractionation in the ^{34}S-^{33}S-^{32}S isotope system. (A) δ^{34}S versus δ^{33}S diagram showing mass-dependent fractionation (heavy line with Δ^{33}S value of 0.0‰), mass-independent fractionation reflected as light lines with variable Δ^{33}S values, and analyses of syn-depositional sulfide and sulfate minerals from > 3.0 Ga sedimentary rocks. (B) Variations in Δ^{33}S of syn-sedimentary sulfur-bearing minerals with geological time. For the purpose this diagram syn-sedimentary minerals includes both syn-depositional and early diagenetic minerals. The gray bar in B encompasses the mean ± one standard deviations of 73 younger (<2.09 Ga) samples. The diagrams shown are the first documenting mass independent fractionation of sulfur isotopes from syn-sedimentary minerals; the data available have expanded by orders of magnitude since the initial study of Farquhar et al. (2000)

absorbs ultraviolet wavelengths of light thought to induce photolytic dissociation of SO_2 (Farquhar et al. 2001). As the concentration of free O_2 (and O_3) gas in the atmosphere prior to the Great Oxidation Event at ∼ 2.42 Ga is thought to have been less than 1 ppm (Catling 2014), there would have been little shielding and photolytic dissociation of SO_2 would have been pronounced (Farquhar et al. 2001). In contrast, the increased shielding of O_2 (and O_3) and/or a decreased concentration of SO_2 in an oxygenated atmosphere after the Great Oxidation Event would have caused photolytic dissociation of atmospheric SO_2, and the mass-independent effects of this reaction, to cease.

Mass-independent fractionation in the S isotope system is measured by the deviation from mass-dependent fractionation. For ^{33}S, this deviation is measured by Δ^{33}S (Eq. 7). As the products (and isotope characteristics) of photolytic SO_2 dissociations in the atmosphere can be "rained out" into the hydrosphere, sedimentary and diagenetic S-bearing minerals may inherit the photolytic isotope signature. As shown in Fig. 3b, prior to the Great Oxidation Event, Δ^{33}S of syn-depositional or diagenetic S-bearing minerals is highly variable, with sulfide minerals (mostly pyrite) having mostly positive Δ^{33}S values and sulfate minerals having negative Δ^{33}S values (cf. Farquhar et al. 2000). This mass-independent fractionation effect is powerful as it can be used to identify S that was present in the atmosphere and hydrosphere during the Archean and trace it through subsequent geological cycles

including tectonic and mineral systems, because it is indelible in younger mass-fractionation processes (LaFlamme et al. 2018a). Examples of how this technique has been used to identify sulfur sources and infer tectonic processes related to ore formation are discussed below.

6.2.3 Kinetic Effects, Thermochemical Sulfate Reduction and Biochemical Sulfate Reduction

Whereas most geochemical reactions occur very rapidly, redox reactions, involving the exchange of electrons, require significant time to occur, particularly at low temperatures (< 200 °C). Ohmoto and Lasaga (1982) were among the first to determine experimentally the rates of redox reactions between aqueous sulfate and aqueous sulfide. They found that at the pH conditions of most hydrothermal systems (4–7) thermochemical sulfate reduction to sulfide involved an intermediate thiosulfate species, and the rate at which thiosulfate formed was the rate-limiting step. Based upon this model they suggested that thermochemical sulfate reduction is an important hydrothermal process only at temperatures above 200 °C.

Subsequent studies have indicated that thermochemical sulfate reduction can be important at temperatures as low as 100–140 °C (Goldhaber and Orr 1995; Machel 2001; Thom and Anderson 2008), particularly when catalysed by the presence of H_2S, certain reactive metals (e.g. Ni, Co, Mn, Cu, Fe, Mg) and organic molecules (Machel 2001; Meshoulan et al. 2016). The isotope effects of thermochemical sulfate reduction depend not only on temperature, but also upon the availability of sulfate. In systems with excess sulfate the kinetic $\Delta^{34}S_{sulfate-sulfide}$ increases with decreasing temperature, from $\sim$ 10‰ at 200 °C to $\sim$ 20‰ at 100 °C (Machel et al. 1995; Meshoulan et al. 2016; and references therein). However, if the supply of sulfate is limited, or if the rate of sulfate supply is less than that of sulfate reduction, all sulfate is reduced to sulfide and $\delta^{34}S$ of the resulting sulfide (either as H_2S in sour gas or as sulfide minerals) approximates the $\delta^{34}S$ value of the original sulfate (Machel et al.

1995). Hence, the absence of significant fractionation between reactant sulfate and product sulfide may indicate limited availability of sulfate in a mineral system.

At lower temperatures (< 100 °C), biochemical sulfate reduction can be an important process to produce H_2S (Goldhaber and Orr 1995; Machel 2001). Due to its importance in a range of ecological and geological processes, including diagenesis, ore formation and sour gas formation, bacterial sulfate reduction has been extensively studied over the last three decades, and the geochemical and isotope effects of this process are well known. At present, sixty genera and over 220 species of sulfur-reducing bacteria are known (Barton and Fauque 2009), and kinetic sulfur isotope fractionation factors have been determined for 32 of these species, covering a large range of environments from freshwater and marine muds, salt lakes, arctic sediments, and hydrothermal environments. Detmers et al. (2001) reported experimental kinetic $\Delta^{34}S_{sulfate-sulfide}$ values of 2.0–42.0‰, and sulfate reduction rates of 0.9–434 fmole/cell/day.[5] These workers noted no correlation between $\Delta^{34}S_{sulfate-sulfide}$ and reduction rates, but found that the largest fractionations were associated with bacteria that completely oxidized electron-donor carbon to CO_2, whereas bacteria that only partially oxidize the carbon (to acetate) produce lower fractionation factors. The four largest fractionation factors (28.5–42.0‰) were produced by bacteria isolated from marine muds (Detmers et al. 2001). When both thermochemical and biochemical sulfate reduction processes are considered, the most extreme fractionations are associated with biochemical sulfate reduction, which Machel et al. (1995) highlighted as one that can be used to distinguish thermochemical (10–20‰) from biochemical sulfate reduction (15–60‰).

In addition, biochemical sulfate reduction appears to have mass-independent fractionation effects, as shown in Fig. 4. This fractionation, which has $\Delta^{36}S/\Delta^{33}S \sim$ -7, was interpreted by Johnston (2011) to indicate biogenic sulfate reduction. This contrasts with the mass-

---

[5] 1 fmole (femtomole) = 10^{-15} mol.

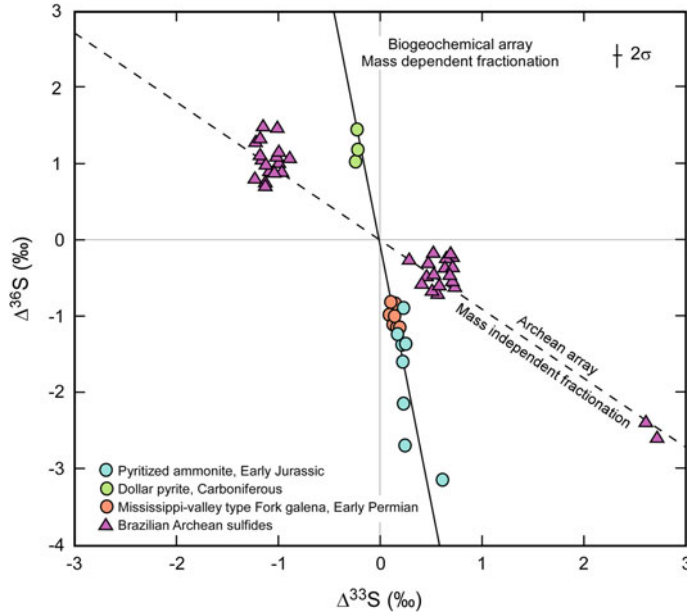**Fig. 4** S isotopic fractionations as measured in situ on the ion microprobe SHRIMP SI. $\Delta^{33}S$ and $\Delta^{36}S$ are the residuals in $^{33}S/^{32}S$ and $^{36}S/^{32}S$ after correction for mass-dependent fractionation (as expressed by $^{34}S/^{32}S$). Of particular significance is the resolution of the Biogeochemical Array (slope -7) from the Archean array (slope -

1) which both can have subpermil anomalies in ^{33}S. Previously, the presence of $\Delta^{33}S$ anomalies alone has been used as a life signal, but in the Proterozoic with potential for Archean inheritance, a complete 4-isotope sulfur analysis is required to understand the origin of the sulfur

independent fractionation signal associated with Archean photolytic dissociation which has $\Delta^{36}S/\Delta^{33}S \sim -1$. Moreover, biogenic mass-independent fractionation is present in Phanerozoic rocks.

Biochemical (bacterial) reduction can also produce significant fractionation in the carbon isotope system. Reduction of acetate and CO_2 to form CH_4 produces significant, but variable fractionation ($\Delta^{13}C_{CO2-CH4}$) of up to 95‰ (Whiticar 1999), with typical fractionation between 25‰ and 60‰ (Conrad 2005). Kennedy et al. (2010) found that carbon associated with bacteriogenic iron oxides was depleted in ^{13}C by up to 22‰, with the greater depletion present in samples more highly enriched in organic carbon. Like biochemical sulfate reduction, the fractionation appears to be highly dependent upon the environment and it is likely to be also dependent upon the species of micro-organism involved.

6.3 Open- and Closed System Fractionation Between Isotope Reservoirs

Many geological processes, particularly devolatilization and degassing, involve the interaction of two distinct geochemical reservoirs. Isotope fractionation between these reservoirs can be modelled using two end-member processes: closed-system, or batch, fractionation, and open-system, or Rayleigh, fractionation. In closed-system fractionation, the two reservoirs are continuously in isotope equilibrium, whereas in open-system fractionation, aliquots of one reservoir are removed and isolated and do not interact with the other reservoir. Batch, or closed-system fractionation (Nabalek et al. 1984) can be modelled according to the relation:

$$\delta_{B,f} - \delta_{B,i} = -(1 - F)1000 \ln \alpha_{A-B} \quad (11)$$

Rayleigh, or open-system, fractionation (Broecker and Oversby 1971) can be modelled according to:

$$\delta_{B,f} - \delta_{B,i} = 1000 \left(F^{(\alpha_{A-B}-1)} - 1 \right) \qquad (12)$$

where $\delta_{B,f}$ is the final isotope composition of reservoir B, $\delta_{B,i}$ is the initial isotope composition of reservoir B, and F is the fraction of reservoir B remaining.

Taylor (1986a) provided a good illustration of the differences between closed- and open-system hydrogen isotope fractionation during the degassing of a magmatic vapor from a magma (Fig. 5). In closed systems (curves a and b) where the vapor remains in contact and in isotope equilibrium with the melt, δD of both reservoirs decrease uniformly as the vapor evolves from the melt. If all hydrogen is extracted into the vapor, the final δD of the vapor is identical to that of the original magma.

In contrast, open-system fractionation (curves c and d) involves continuous removal and isolation of aliqots of evolved vapor from the magma, with the aliquots equilibrating with the magma only prior to removal. As a consequence, the δD characteristics of the magma and evolved vapor decrease dramatically as the amount of H_2O remaining in the magma (F) decreases (Taylor 1986a). Individual aliquots of vapor produced during open-system magma degassing can have dramatically lighter
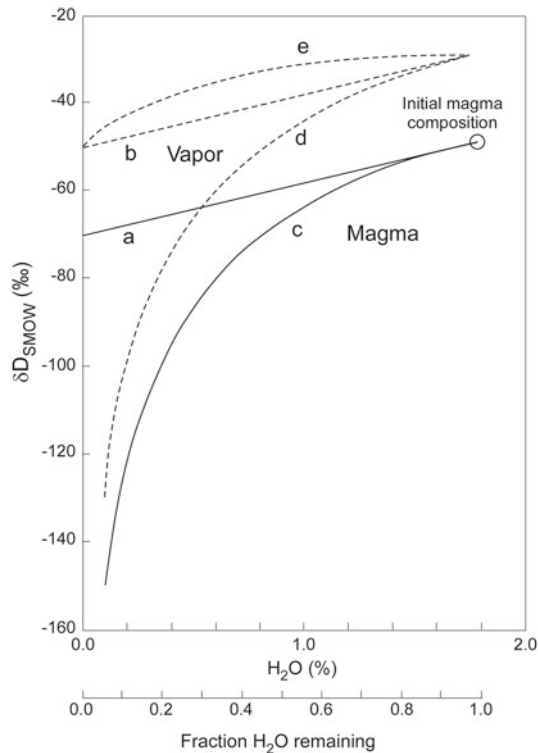

Fig. 5 Hydrogen isotope shifts in magmatic vapor and magma in hypothetical models of closed-system (batch) degassing (curves a and b), and open-system (Rayleigh) degassing (curves c and d; curve e indicates the accumulated magmatic vapor). The solid lines indicate modelled composition of the residual magma, and the dashed lines indicate modelled composition of the evolved vapor. The initial magma had $\delta D = -50‰$ and $[H_2O] = 1.9\%$; a value for 1000 ln $\alpha_{\text{vapor-melt}}$ of 20‰ was used. Reproduced with permission from Taylor (1986a); Copyright 1986 Mineralogical Society of America
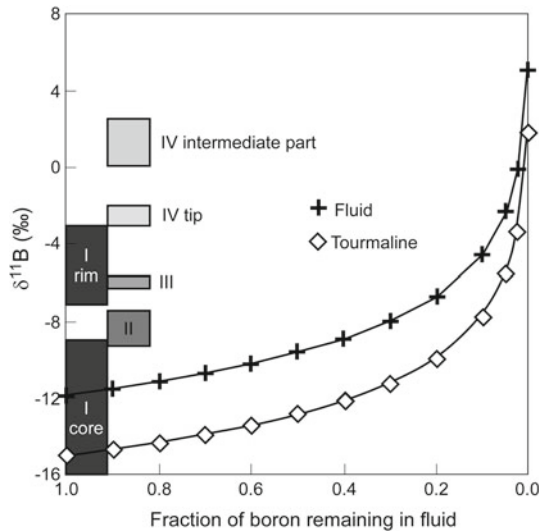
Fig. 6 Rayleigh fractionation model to explain boron isotope zoning in tourmaline from the Teremkyn gold deposit, Darasun district, eastern Russia (modified after Baksheev et al. 2015). The initial boron (12‰) is interpreted to be granite-derived (i.e., stage I core) while the composition of later tourmaline (stage I rim and stages II to IV) reflects Rayleigh fractionation driven by tourmaline crystallization (Baksheev et al. 2015)

δD than fluids produced during closed-system degassing, particularly as degassing proceeds towards completion. However, the accumulated vapor produced by open-system degassing has a much more moderate evolution (curve e), not dissimilar to that produced by closed-system degassing.

Open- vs. closed-system fractionation has also been demonstrated for the boron isotope system. In this case, the fluid-vapor fractionation is generally insignificant (only about 1 ‰ at 400° C: Kowalski and Wunder 2018) but fluid-mineral fractionation is strong owing to the contrasting coordination environment of the boron ion in aqueous fluid versus solid phases. Furthermore, in the case of tourmaline or other B-rich minerals, crystallization can strongly deplete the fluid reservoir in boron, so that Rayleigh fractionation is a common process. This was demonstrated in controlled experiments by Marschall et al. (2009) and Rayleigh fractionation has been invoked to explain systematic core-rim isotope variations in zoned tourmaline from hydrothermal ore deposits in several studies (e.g., Baksheev et al. 2015, Fig. 6).

7 Light Stable Isotope Characteristics of Major Geological Reservoirs

Ore fluids in mineral systems have a number of different sources and they carry metals, sulfur, carbon, boron, chlorine and other components that have been sourced from many different geochemical reservoirs. Stable isotope studies are one of very few tools to determine these sources as the reservoirs commonly (although not always) have distinctive stable isotope signatures. Figure 7 and Table 2 summarizes the isotope characteristics of a range of natural reservoirs. Figure 8a illustrates the characteristics of different crustal fluids on a $\delta^{18}O$ versus δD diagram, and Fig. 8b shows a similar plot of $\delta^{11}B$ versus δD used by Adlakha et al. (2017) to distinguish fluid sources of the McArthur River U deposit. Huston and Champion (2023), Lobato et al. (2023), Mathur and Zhao (2023) and Wilkinson (2023) discuss how radiogenic lead isotopes and heavy stable metal isotopes can be used to infer metal source.
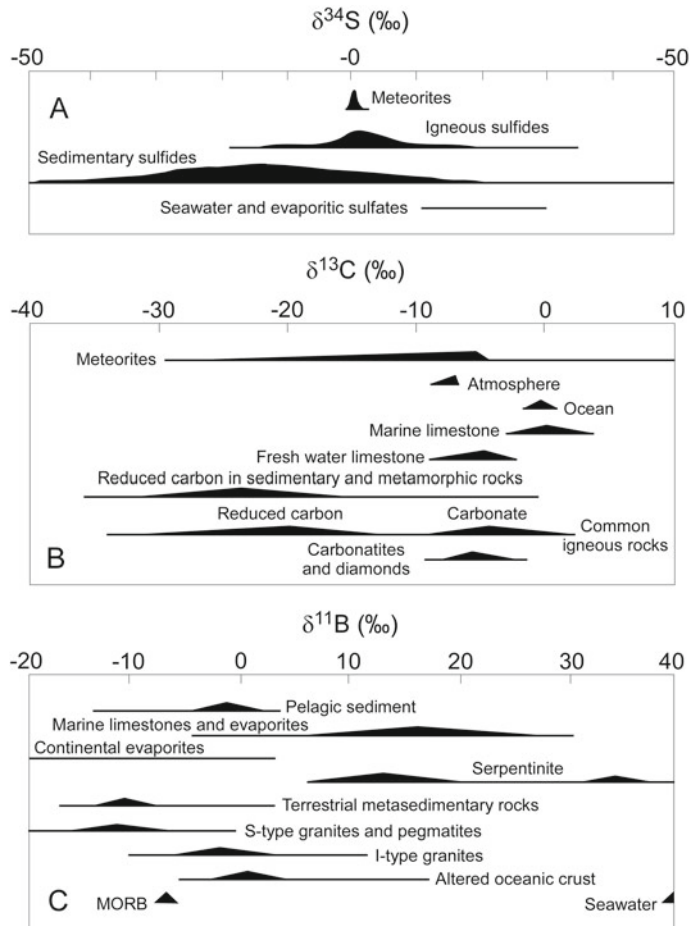
Seawater is one of the major Earth reservoirs and it plays a key role in metallogenetic models for a range of stratiform ore deposit types. Modern ocean water has H- and O-isotope compositions identical to V-SMOW, and it is thought to have been relatively uniform through time, with ranges in δD and $\delta^{18}O$ of -25‰ to 0‰ and -3‰ to 0‰, respectively, since the Archean (Sheppard 1986). Seawater also has a uniform and distinctly heavy boron isotope composition ($\delta^{11}B \sim 40$ ‰) compared to all other Earth reservoirs (Table 2), which allows to distinguish marine and terrestrial provenance of boron in ore fluids and the minerals derived from them (e.g., Xavier et al. 2008). The H- and O-isotope composition of seawater is also the fundamental basis of the meteoric water line, an important reference on plots of H- and O-isotope compositions

(Fig. 8a). The meteoric water line (Craig 1961) is defined by:

$$\delta D = 8\delta^{18}O + 10 \qquad (13)$$

The isotope composition of meteoric water is governed by that of seawater and the temperatures of seawater evaporation and precipitation from clouds, both of which are related to latitude and altitude. Lower values of δD and $\delta^{18}O$ are characteristic of higher latitude and altitude (Sheppard 1986).

Traditionally, formation waters in sedimentary basins were thought to be seawater or brine entrained in sediments at the time of deposition (i.e. connate waters), but subsequent work has demonstrated that many (or most) formation waters are meteoric waters that infiltrated into

**Table 2** Range in stable isotope values of the mantle and common upper-crustal sedimentary and igneous rocks

Reservoir	δD	$\delta^{18}O$	$\delta^{11}B$	$\delta^{13}C$	$\delta^{34}S$
Upper mantle	−80‰ to -50‰ for upper mantle; −46‰ to −32‰ for subduction-modified mantle	5.7 ± 0.3‰; 6.0–6.7‰ for subduction-modified mantle	7.1 ± 0.9 ‰ for MORB-source upper mantle	∼ -5‰	0–1‰ (based on mantle xenolith data; overlaps with meteoritic data)
Upper crustal sedimentary rocks					
Psammitic rocks	—	8–15‰	--	—	−70‰ to 70‰
Pelitic rocks	−90‰ to −40‰	13–20‰	−13 to 4 ‰ for pelagic clays, continental metapelites mostly less than -10 ‰	−30‰ to −15‰ (reduced carbon)	
Limestone and chert	—	25–35‰	−5 to 26 ‰ for marine carbonates, mostly above 5; −12 to 8 for chert	0 ± 5‰	
Upper crustal igneous rocks					
Felsic rocks	−130‰ to −40‰ (this range is interpreted to be the result of Rayleigh degasing, with highest δD values associated with the least degased samples, as indicated by whole-rock H_2O content)	Mostly 6–10‰	−2 ± 5 ‰, rarely below -8 ‰ for I-type rocks; -11 ± 4 ‰, rarely above -8 ‰ for S-type felsic rocks	−35‰ to −10‰ (reduced carbon; −10‰ to 3‰ (oxidized carbon)	Mostly -5‰ to 10‰, but total range from −20‰ to 25‰
Mafic rocks	−120‰ to 0‰ (total range); −85‰ to −75‰ (primary magmatic composition of oceanic basalt)	4.9–8.0‰	−7.1 ± 0.9 ‰ for fresh MORB, −2 to 17 ‰ for altered basalt, gabbro in ophiolites, −3 to −12 ‰ for fresh OIB, higher values if seawater altered	−29.5‰ to −3.5‰ (total range); −11‰ to −3.5‰ for carbon extracted above 600 °C (the most likely magmatic range; most data cluster near -5‰,)	−3.0‰ to 2.5‰ (tholeiites); 2.5‰−6.0‰ (alkali basalts)

Data from Ohmoto and Rye (1979), Kyser (1986), Taylor and Sheppard (1986), Hoefs (1997) and Marschall and Foster (2018). In most cases metamorphosed rocks retain the isotope characteristics of their precursors (see text)

sedimentary basins subsequent to deposition and diagenesis (Kharaka and Hanor 2003). Evidence for this interpretation stems in part from isotope arrays in $\delta^{18}O$ versus δD plots that trend toward the meteoric water line and are consistent with the composition of meteoric fluids at likely recharge zones (see Kharaka and Hanor 2003 for discussion). On the other hand, some basins contain formation waters that are interpreted as true connate waters. As these connate waters were originally derived from seawater, their isotope signature should reflect that of seawater at the time of sedimentation (Sheppard 1986). Figure 8a indicates that connate waters, including evaporative brines, are characterized by δD and $\delta^{18}O$ values somewhat lower and higher, respectively, than modern seawater. These data from Gulf coast basins in the United States

Fig. 8 Variations in stable
isotope characteristics of
fluids present at the Earth's
surface or in upper crustal
rocks. A. $\delta^{18}O$-δD diagram
showing isotope
characteristics of common
crutal fluids. Data from Taylor
(1979) and Kharaka and
Hanor (2003). B. Variations
in $\delta^{11}B$ (modified after
Adlakha et al. 2017)
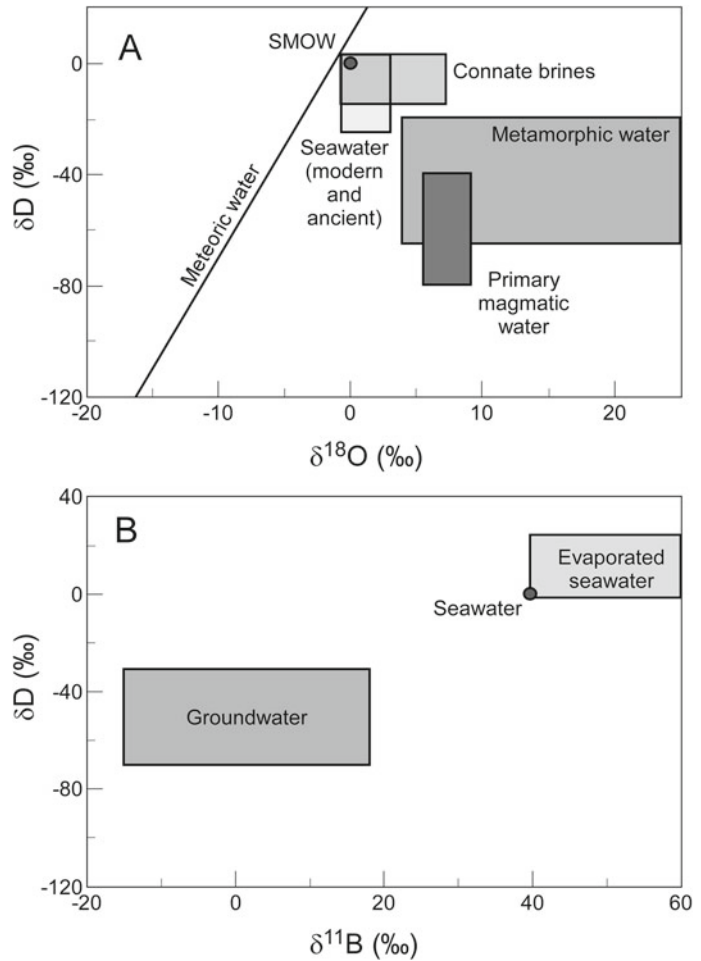
(Kharaka and Hanor 2003, and references therein), indicate a slight shift from oceanic water, possibly due to equilibration with the host rocks. Although limited, the data suggest that connate fluids may have a distinctive δD - $\delta^{18}O$ signature relative to meteoric water and other crustal fluids. Marine-derived connate fluids should also have a distinctive $\delta^{11}B$ signature relative to crustal fluids because of the uniquely high $\delta^{11}B$ value of seawater. This was used with success in studies of B-isotopes in tourmaline from U-deposits of the Athabasca Basin by Mercadier et al. (2012) and Adlakha et al. (2017) as shown on Fig. 8b.

The stable isotope composition of the upper mantle and mafic igneous rocks derived from it are thought to be relatively homogeneous, with

$\delta^{13}C \sim$ -5‰, $\delta^{18}O \sim 5.7 \pm 0.3$‰, $\delta^{34}S \sim$ 0–1‰ (with $\Delta^{33}S$, $\Delta^{36}S \approx 0$) and $\delta^{11}B \sim 7 \pm 1$ ‰ (Table 2). The exception to this is where such rocks are altered on the seafloor or, in the case of arc settings, where the upper mantle is hydrated from slab-released fluids. The homogeneity of mantle-derived rocks contrasts with crustally-derived rocks, which are more variable (Fig. 7) due to the wider range of source components involved and to the number of chemical processes (metamorphism, melting, alteration and weathering) which cause isotope fractionation, particularly in the upper crust, atmosphere and hydrosphere. For example, siliciclastic sedimentary rocks have higher $\delta^{18}O$ values than igneous rocks from which they were derived due to fractionation during low temperature erosion and

chemical weathering. Sedimentary rocks also have a wide range in $\delta^{13}C$ and $\delta^{34}S$ values (Table 2) due to biological processes and low-temperature, disequilibrium fractionation as discussed above, and their $\delta^{11}B$ values depend on their marine or terrestrial provenance (Table 2). The O-isotope discrimination of sedimentary versus igneous (juvenile, arc-related) sources of granites is well established (Taylor and Sheppard, 1986). Trumbull and Slack (2018) showed that the $\delta^{11}B$ composition of granites and related volcanic rocks also reflects the S- and I- type source dichotomy (see Table 2). The relatively heavy boron in I-type, continental arc magmas ($\delta^{11}B$ from -10‰ to 12‰, average -2‰), relates ultimately to seawater alteration of the sub-arc magma source, whereas the lighter boron in S-types ($\delta^{11}B$ from -22‰ to 0‰, average $\sim$ -11‰) is due to continental (meta)sedimentary rocks in the source.

In cases where magmas were derived by partial melting of hydrothermally altered rocks (Muehlenbachs et al. 1974; Taylor 1986b), the $\delta^{18}O$ signature shifts, commonly to lower values as seen in igneous rocks from Iceland (Muehlenbachs et al. 1974) and the Yellowstone complex in Wyoming, USA (Friedman et al. 1974; Hildreth et al. 1984). Schmitt and Simon (2004) attributed the same effect of hydrothermal alteration of the magma source to explain $\delta^{11}B$ variations in volcanic rocks from the Long Valley caldera.

7.1 The Effects of Metamorphism, Metasomatism and Devolatilization

Metamorphism of a rock can change its stable isotope characteristics through two broad processes, devolatilization or the influx of exogeneous fluids. Devolatilization is the generic process whereby volatile components of a rock are lost during prograde metamorphism and includes dehydration, decarbonation and desulfidation. In some mineral systems, orogenic gold systems, for example, metamorphic fluids produced by these processes are thought to be ore fluids (e.g. Phillips and Groves 1983).

The most important devolatilization reaction is dehydration. According to Wedepohl (1969a) and Engel and Engel (1958b), the average water content of pelitic rocks decreases up metamorphic grade from 5.0% in shales, to 2.96% in phyllites and slates, to 2.41% in mica schists, to 2.02% in sillimanite gneisses, and to 0.62% in transitional amphibolite-granulite facies semipelitic rocks. On an atomic basis, metamorphic dehydration will remove at most 10% of oxygen, but up to 100% of the hydrogen if the process goes to completion. As a consequence, the effect on isotope composition is minor for oxygen (at most an increase in $\delta^{18}O$ of 0.6‰: Valley 1986), but can be significant for hydrogen (decreases in δD of up to 16‰ or 40‰, depending upon the process of devolatilization assumed: Valley 1986). As the water content in sandstone and igneous rocks is much lower than in pelitic rocks (Wedepohl 1969a,b), the effect of metamorphism on oxygen and hydrogen isotope characteristics of these rocks is much less. Hence, for most siliciclastic and igneous rocks, $\delta^{18}O$ of the metamorphosed rock is similar that of the protolith, but δD can significantly different.
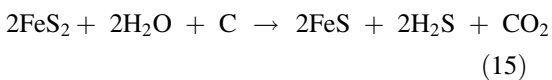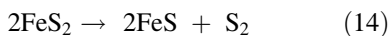
Boron in clastic sedimentary rocks is hosted mainly in clays and micas (Trumbull and Slack 2018) and the breakdown of these hydrous minerals during metamorphism generally releases boron to the metamorphic fluid (Moran et al., 1992). At the same time, the B-isotope fractionation between sheet silicates and hydrous fluid causes a progressive lowering of $\delta^{11}B$ values in the higher-grade rocks and the opposite effect for the fluid phase. The situation changes if tourmaline forms during metamorphism because it has a high thermal stability and preserves the boron content in the rock, and its B-isotope composition, during prograde metamorphism (Trumbull and Slack 2018).

Decarbonation reactions can cause significant changes in both $\delta^{13}C$ and $\delta^{18}O$. Metamorphism and devolatilization of marly carbonate rocks commonly produces calc-silicate rocks containing wollastonite (after marly limestone) or diopside (after marly dolostone). Both of these reactions produce CO_2 as a product, which then escapes. Valley (1986) summarized the isotope
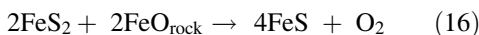
effects of contact metamorphism on carbonate rocks, indicating isotope shifts of up to 14‰ in $\delta^{13}C$ and 22‰ in $\delta^{18}O$, although these shifts were spatially restricted to within 3 km of the causative granite. These shifts in skarns and marbles related to igneous intrusion require that the magmatic-hydrothermal fluids present also experienced significant isotope shifts during decarbonation reactions.

During regional metamorphism, shifts in $\delta^{13}C$ and $\delta^{18}O$ are likely to be restricted. Valley (1986) showed that steep isotope gradients are present at the contacts between compositionally and isotopically distinct units, whereas within these units the isotope signature is uniform. Based on this he suggested that regional metamorphism does not affect the isotope characteristics of the protolith unless significant, channelized fluid flow occurred. However, under situations involving the influx of isotopically distinct exogeneous fluids, isotope shifts in δD, $\delta^{13}C$ and $\delta^{18}O$ can occur. In contrast to the C, O and H isotope systems, the variation of rock $\delta^{11}B$ values during prograde metamorphism can vary strongly depending on the specific mineral assemblage and reactions involved (Trumbull and Slack 2018 and references therein).

Studies by Ferry (1981), Pitcairn et al. (2010), Zhong et al. (2015) and Finch and Tomkins (2017) have indicated that as temperatures increase during regional and contact metamorphism, pre-existing pyrite converts to pyrrhotite according to one or more of the following (or similar) reactions:

$$2FeS_2 \rightarrow 2FeS + S_2 \qquad (14)$$

$$2FeS_2 + 2H_2O + C \rightarrow 2FeS + 2H_2S + CO_2 \qquad (15)$$

Or

$$2FeS_2 + 2FeO_{rock} \rightarrow 4FeS + O_2 \qquad (16)$$

The first two reactions are desulfidation reactions in that sulfur is lost from the rock, but the last reaction does not involve sulfur loss. The above studies indicate that the metamorphic conversion

of pyrite to pyrrhotite occurs over a temperature range of 200 °C to 550 °C. Graphical analysis of whole rock geochemical data by Ferry (1981) suggested that reactions similar to (15) are the most likely reactions for pyrite to pyrrhotite conversion and require fluid influx from metamorphic dehydration reactions or from external sources.

The isotope effects of pyrite breakdown during prograde metamorphism are not well studied, with the best example being a laser ablation study by Alirezaei and Cameron (2001) who found no statistically significant fractionation between pyrite and pyrrhotite or between metamorphic zones. They interpreted these results to indicate that the conversion of pyrite to pyrrhotite involved uptake of iron from wall rocks (i.e. reaction 16) rather than sulfur loss. However, at temperatures of 300–450 °C, conditions where the conversion of pyrite to pyrrhotite is greatest (Ferry 1981), $\Delta^{34}S_{pyrite-H2S}$, $\Delta^{34}S_{pyrrhotite-H2S}$ and $\Delta^{34}S_{pyrite-pyrrhotite}$ are 0.8–1.2‰, 0.2–0.3‰ and 0.6–0.9‰, respectively. This suggests that $\delta^{34}S$ variations caused by metamorphic desulfidation are likely to be small, probably not recognizable given the large variations in $\delta^{34}S$ that characterize sedimentary pyrite. Moreover, the isotope composition of sulfur in metamorphic fluids is likely to be similar to that of the rocks that evolve the fluid.

Because primary metamorphic fluids cannot be sampled at or near the Earth's surface, their isotope composition has been inferred using the isotope, mineralogical and chemical composition of metamorphic rocks with estimates of fractionation factors at the temperature range characteristic of metamorphism. Due to the large range in the isotope composition of the protoliths and the range of metamorphic temperatures, the inferred isotope field of metamorphic fluids is large (Fig. 8). Despite this, metamorphic fluids have distinctive isotope characteristics relative to meteoric water, seawater and connate brines, although they overlap with the field of magmatic fluids.

The isotope composition of magmatic fluids also has been estimated from the isotope and

chemical composition of igneous rocks and minerals, combined with crystallization temperatures and isotope fractionation factors (e.g. Taylor 1979; Sheppard 1986). The resulting field is large, although not as large as the metamorphic fluid field, with which it largely overlaps. Unlike metamorphic fluids, magmatic fluids have a distinctive isotope signature relative to other fluids such as seawater, basinal brines and meteoric waters present in the upper part of Earth's crust. It must be stressed that the isotope fields shown in Fig. 8 are for primary fluids. Reaction of these fluids with rock has the potential to shift the isotope composition of the fluid, particularly under rock-dominated conditions.

8 Applications of Light Stable Isotopes to Ore Genesis Studies and Exploration

As discussed above, light stable isotopes fractionate during a range of geological processes, hence variations in stable isotope ratios can be used to track these processes. Moreover, isotope data can provide information as to the temperatures and pressures at which mineral systems evolve, and the sources of fluids. The following section discusses how stable isotope data can be used to constrain these processes and conditions of ore formation. More importantly, it also discusses the limitations and ambiguities of some of these constraints.

8.1 Geothermometry and Geobarometry

Temperature, redox state, salinity and pH of the ore fluid largely determine what metals can be transported and how these metals can be deposited. These parameters can be determined from mineral assemblages, but also from fluid inclusion and stable isotope data. Due to temperature-dependent fractionation of stable isotopes between minerals (Fig. 1), the temperature of deposition can be estimated from $\Delta^{34}S$, $\Delta^{18}O$ and $\Delta^{13}C$ data. However, use of these parameters for

geothermometry makes several implicit assumptions: (1) the minerals precipitated at the same time from an isotopically homogeneous fluid, (2) the fractionation between minerals has not been affected by later geological events, and (3) isotope fractionation between minerals occurred under equilibrium conditions. The first two assumptions can be largely (but not entirely) assessed by paragenetic studies, and at higher temperatures (>300 °C), disequilibrium becomes less important in most systems (see below).

Another factor that must be considered in assessing isotope thermometers is the purity of mineral separates analysed. Cross-contamination of mineral separates results in temperature estimates that are too high. For example, a hypothetical fluid with $\delta^{18}O$ of 8.0‰ will precipitate quartz and magnetite with $\delta^{18}O$ values of 17.4‰ and -1.5‰ at 250 °C, respectively, giving a $\Delta^{18}O_{quartz-magnetite} = 18.9$‰. If the two separates are cross-contaminated by 10% (based on atomic oxygen), the impure quartz and magnetite separates will have with $\delta^{18}O$ values of 15.5‰ and 0.4‰, respectively, giving a $\Delta^{18}O_{quartz-magnetite} = 15.1$‰, which corresponds to a temperature of 265 °C, which is 15 °C higher than the hypothetical conditions. This effect becomes stronger at higher temperature and with greater cross contamination. Hence, care must be taken to ensure sample purity, and temperatures estimated from isotope mineral pairs should be considered maximum temperatures. In-situ techniques like SIMS can solve many of the impurity issues, but at the cost of a larger analytical uncertainty, which equates to a larger temperature error.

If three or more minerals have been deposited concurrently from an isotopically homogeneous fluid, determining ΔX values for mineral pairs can be used to assess the reliability of the isotope thermometry. Determining δX of three coexisting minerals yields three separate ΔX and temperature estimates, and if all three temperature estimates are within error, greater confidence can be placed in the overall temperature estimate. If the temperatures differ, the mineral assemblage may not have formed concurrently under equilibrium conditions, or one or more minerals have

been affected by post-depositional disturbance, or the mineral separates are not pure.

The uncertainties in stable isotope geothermometry depend on the relative uncertainties in determining δX. If the (2σ) uncertainties associated with δX for each mineral pair are similar, the (2σ) uncertainty in ΔX is $\sqrt{2} \times 2\sigma_{\delta X}$; if the uncertainties in δX are dissimilar, the uncertainty is ΔX is estimated by adding the individual uncertainties in δX in quadrature. This uncertainty in ΔX is then used to estimate the uncertainty in temperature. Note that the temperature uncertainty is asymmetric, with the lower-temperature uncertainty smaller than the higher-temperature uncertainty. This is because the intensity of fractionation in most stable isotope systems decreases with increasing temperature.

Once a temperature estimate has been made, it can be used to constrain other characteristics of the mineral system. Possibly the most important of these is the isotope characteristics of the ore fluid, which is calculated from temperature-dependent fluid-mineral fractionation factors. If sufficient data are available, estimates of δD_{fluid}, $\delta^{11}B_{fluid}$, $\delta^{13}C_{fluid}$, $\delta^{18}O_{fluid}$ and $\delta^{34}S_{fluid}$ can be made, which is very useful information for determining fluid sources. Furthermore, isotope temperature determinations can be combined with fluid inclusion data to estimate the pressure and, thereby, crustal depth at which mineralization occurred. The pressure can be estimated using the following equation:

$$P_t = P_h + (T_t - T_h)(\Delta P/\Delta T) \qquad (17)$$

where P_t is the trapping (geological) pressure of the fluid inclusion, P_h is the homogenization pressure (determined from fluid composition and T_h), T_t is the trapping (geological) temperature of the fluids (determined from isotopic data as described above or from another independent geothermometer), T_h is the fluid inclusion homogenization temperature, and $\Delta P/\Delta T$ is the slope of the isochore. Examples where this methodology has been applied include Huston et al. (1993) Honlet et al. (2018), and many others.

8.2 Tracking Fluid Sources

Stable isotopes are a powerful tool to determine the source of water in ore fluids, and, to a lesser extent the sources of boron, sulfur and carbon within them. As discussed earlier, many fluids present in the upper crust have quite distinctive isotope characteristics, which enables inference of the type of fluid from which the ore fluids were derived (see Fig. 8). An example is the strong contrast between the $\delta^{11}B$ values of seawater, marine carbonates and evaporitic rocks of marine origin on the one hand, and their equivalents from terrestrial, continental settings on the other (see Fig. 7). Thus the values of $\delta^{11}B$, $\delta^{34}S$ and $\delta^{13}C$ can be indicative of source (Fig. 7, Table 2), but because there is considerable overlap between potential reservoirs, in many (most) cases, the isotope signature of the ore and gangue minerals is not definitive of a particular source.

An important exception to this generalization for the sulfur isotope system is the use of multiple sulfur isotope ratios to identify mass-independent fractionation. The recognition of photolytic mass-independent fractionation of sulfur isotopes prior to the Great Oxidation Event (Farquhar et al. 2000, 2001) has opened a totally new method to identify the relative importance of sulfur that has or has not interacted with the atmosphere or hydrosphere, particularly in Archean and earliest Paleoproterozoic mineral systems. This tool is particularly useful for systems in which the source of sulfur is contested, for example volcanic-hosted massive sulfide mineral systems (Huston et al. 2023), orogenic gold deposits (LaFlamme et al. 2018b) and orthomagmatic Ni-Cu-PGE deposits. In the latter, one mechanism that has been proposed to produce an immiscible Ni-Cu-PGE sulfide melt from the parental mafic/ultramafic magmas is sulfur saturation of the magma by ingestion of sulfide-rich wall rocks (Lesher and Campbell 1993). As many of these deposits formed in the Neoarchean, the distinctive signature of mass-independent sulfur isotope fractionation can distinguish between mantle and crustal and mantle

sulfur.[6] Bekker et al. (2009), Ding et al. (2012) and Fiorentini et al. (2012) used $\Delta^{33}S$, which indicates the presence ($|\Delta^{33}S| > 0.0‰$) or absence ($\Delta^{33}S \sim 0.0‰$) of crustal sulfur, to indicate that sulfur contamination from the crust was an important process in some, but not all, orthomagmatic Ni-Cu-PGE deposits, and that the presence of mass-independent fractionation may be a signature of the larger deposits (Fiorentini et al. 2012).

8.3   Tracking Geochemical Processes

One of the more powerful uses of stable isotopes in mineral systems studies is identifying and then tracking geochemical processes like redox reactions and phase separation (boiling, magma degassing). As discussed above, many geochemical processes cause significant, and, in some cases, diagnostic, isotope shifts in rocks and/or minerals, or cause spatial or temporal isotope gradients. These effects are most easily observed where there are strong isotope contrasts between the reactants and the products of the geochemical reaction. For example, in volcanic-hosted massive sulfide systems, evolved seawater, the main ore fluid, has hydrogen and oxygen isotope characteristics that contrast with the rocks and other potential fluids that it interacts with. As a consequence, hydrolytic alteration zones developed in these systems can be easily mapped using whole-rock $\delta^{18}O$ data, and the involvement of other fluids (e.g. magmatic-hydrothermal) can be assessed (Huston et al. 2011, 2023; and references therein).

One of the earliest uses of oxygen and hydrogen isotopes in alteration studies was determining the interaction of magmatic-hydrothermal ore fluids and meteoric water with host rocks in porphyry copper mineral systems. Sheppard et al. (1969, 1971) showed that hydrothermal minerals from core potassic alteration zones in these deposits formed from

magmatic-hydrothermal fluids, whereas clay minerals in peripheral argillic alteration zones formed from heated, overprinting meteoric water. These isotope data were one of the key datasets in establishing the porphyry copper genetic model in the 1960s and 1970s, and the results of Sheppard et al. (1969, 1971) have been confirmed by studies of porphyry systems of different ages around the world.

Boron isotope studies of ore systems have focussed on tourmaline because this mineral is common, resists alteration, preserves zoning and contains percent levels of boron, but other minerals may become important (e.g. white mica, see "future directions"). One of the first uses of B-isotopes to understand ore fluid sources was the study of massive sulfide deposits associated with tourmalinite by Palmer and Slack (1989) and the method grew rapidly since the advent of in-situ studies using SIMS or LA-ICPMS (see Slack and Trumbull 2011; Trumbull et al. 2020). Common applications have been to constrain the fluid source or to define mixing of multiple sources and their temporal relationships. For example, Xavier et al. (2008) found distinctly high $\delta^{11}B_{tourmaline}$ values ($> 10‰$) that indicate a marine origin for high-salinity ore fluids in Brazilian IOCG deposits. Zoning and replacement textures combined with in-situ B-isotope ratios tracked fluid evolution and mixing (Pal et al. 2010; Baksheev et al. 2015; Lambert-Smith et al. 2016). In granite-related Sn-W deposits and pegmatites, tourmaline B-isotope studies have been used to recognize the magmatic-hydrothermal transition by its effect on B-isotope partitioning (e.g. Drivenes et al. 2015; Siegel et al. 2016).

Rotherham et al. (1998) interpreted large variations in $\delta^{34}S_{sulfide}$ to be indicative that reduction of an originally highly oxidized ore fluid by interaction with ironstone was the depositional mechanism for the Starra (now known as Selwyn) copper–gold deposit in northwest Queensland, Australia. Large (1975) and Huston et al. (1993) interpreted zonation in $\delta^{34}S_{sulfide}$ data from ironstone-hosted deposits in the Tennant Creek district in a similar manner. Large variations in $\delta^{34}S$ data can be indicative of

---

[6] In this case, defined as sulfur that has (crustal) and has not (mantle) interacted with the atmosphere prior to the Great Oxidation Event at $\sim$ 2420 Ma.

redox reactions and spatial and temporal gradients can be used to track and map the progression of these reactions.

Pyrite- and sulfate-bearing advanced argillic alteration assemblages form by two processes in the porphyry-epithermal mineral system: (1) disproportionation of magmatic SO_2 to form aqueous H_2S and sulfate, and (2) condensation of hydrothermal H_2S into oxidized groundwater followed by oxidation of the H_2S to form sulfate. Both of these processes produce sulfuric acid, which reacts with rock to produce pyrophyllite and/or kandite (a complex mixture of members of the kaolinite-nacrite-dickite family), which characterize advanced argillic assemblages. These two processes, which occur in different parts of the porphyry-epithermal system, can produce mineralogically similar alteration assemblages that are difficult to distinguish. Comparison of sulfur isotope data from sulfide and sulfate minerals is one method of distinguishing between them (Rye et al. 1992). Rye (2005) found that because SO_2 disproportionation is a high temperature process, it produces equilibrium isotope fractionation, whereas oxidation of H_2S in groundwater, a low temperature process, generally produces disequilibrium isotope fractionation between sulfide and sulfate minerals. These characteristics, combined with other mineralogical data can be used as criteria to distinguish between SO_2 disproportionation and the oxidation of aqueous H_2S in groundwater as mechanisms to form advanced argillic alteration assemblages.

In summary, variations in stable isotope ratios can be used to identify and track geochemical processes in mineral systems. It must be stressed, however, that stable-isotope signatures can be affected by many geochemical processes, and these signatures are rarely diagnostic of one process alone. As an example, the presence of a $\delta^{34}S_{sulfide} \sim 0‰$ is commonly taken to indicate that the sulfur was derived (directly) from a magma. However, this signature can be produced by the fortuitous mixing of two non-magmatic sources, or by leaching of volcanic rocks, which would have a similar signature. Hence, when interpreting isotope data (and geochemical data in general) all processes that produce an isotope signature must be considered valid, and not just the favoured process the signature "proves". It is rare that an isotope signature is sufficiently unique to eliminate all but one process as its cause. The non-uniqueness of isotope signatures can, in some cases, be overcome by the use of multiple isotope systems, including both stable and radiogenic isotopes (see future directions).

8.4 Exploration and Discovery

Although stable isotopes have proved to be extremely useful in understanding fluid sources and processes that form ore deposits, discoveries of deposits using isotope data are uncommon. Two examples that we are aware of are the discovery of a new skarn lens in the Kamioka district in Japan using $\delta^{18}O$ data of carbonate minerals (Naito et al. 1995), and the discovery of the West 45 lens at the Thalanga volcanic-hosted massive sulfide deposit in Queensland, Australia using whole-rock $\delta^{18}O$ data (Miller et al. 2001). Despite well-documented and consistent zonation of isotope values for a number of deposit types (see above and later papers in this volume), isotope methods for exploration have not been taken up by industry to any significant extent. Barker et al. (2013) attribute the lack of uptake by industry to: (1) the costs of analyses, (2) the requirement of specialist analytical labs, and (3) the slow turnaround time for analyses. They noted that for isotopes to be taken up by industry, the quantity of analyses on a project would need to increase from the tens or hundreds typical for ore genesis studies to thousands for exploration. Barker et al. (2013) reported a study in the Carlin district, Nevada, USA in which they used large numbers of analyses to show decrease in $\delta^{18}O$ of carbonate minerals towards the Screamer gold deposit. Because of the large variability of the data at the drill hole scale, the statistical robustness of large data sets was required to document this zonation. Hence, uptake of stable isotope variations as an exploration tool will require a reduction in the costs and time required for analyses, and a greater number of laboratories able to provide them.

9   Future Directions

As with other science fields, the techniques and interpretations of stable isotopes in metallogenic studies evolve over time. Techniques being developed at present could strongly influence the future direction of stable isotope research in metallogenic studies. These include the development of new techniques (e.g. clumped isotopes), the ability to integrate data from different isotope systems (both stable and radiogenic) on the same rock, mineral or spot, and the increasing capability for inexpensive and rapid analyses.

Like the discovery of significant mass-independent sulfur isotope fractionation in the Archean, the development of analytical techniques to measure fractionation of clumped isotopes has the potential to provide a new tool to understand ore genesis. Rather than considering variations in the isotope abundance of an individual element, clumped isotopes measurements identify isotope variations in molecules. For example the CO_2 molecule can vary in atomic mass from 44 to 49, with mass number 44 ($^{12}C^{16}O_2$) being the most abundant (98.40%) and mass number 49 ($^{13}C^{18}O_2$) the least (44.5 ppb) (Eiler 2007). Just like isotopes, these ``isotopologues'' also fractionate with temperature (Ghosh et al. 2006). At present, clumped isotope geochemistry has been extensively used in paleoenvironmental, paleobiological and related studies (Huntington et al. 2011; Eagle et al. 2011), but the application to fluid flow and metamorphism (Swanson et al. 2012; Lloyd et al. 2017) suggest that they might also be useful in ore genesis studies where they can determine the temperature and isotope (i.e. $\delta^{18}O$) composition of ore fluids (Mering et al. 2018). Clumped isotopes may be particularly useful in low temperature systems, such as those hosted in basins, where estimating temperature and determining the origin of fluids are problematic. Interpretation of these data does not require knowledge of other information such as salinity and the isotopic signature is less susceptible to later alteration.

To date, the application of B-isotope studies of ore deposits has been almost exclusively based on tourmaline (Trumbull et al. 2020). White mica has been targeted before in studies of metamorphism (Konrad-Schmolke and Halama 2014), but it is virtually unexplored in ore deposit studies even though mica, particularly white mica, contains the highest concentrations of boron of all common rock-forming minerals (Harder 1974). White mica is even more common than tourmaline in alteration zones, and in cases where both minerals coexist, the difference in fluid-mineral B-isotope fractionation between them can be used for geothermometry. A case study of the Panasqueira Sn-W deposit by Codeço et al. (2019) showed that mineralization temperatures derived from $\Delta^{11}B$ in coexisting mica and tourmaline are consistent with other geothermometers and can be used to track cooling of the mineralizing system.

The development of microanalytical methods of isotope analysis has allowed for the first time determination of a large suite of isotope ratios, both stable and radiogenic, from essentially the same spot or the same mineral. Integration of such information can lead to conclusions that are more robust and far reaching than conclusions from each isotope system individually. A good example of this is the microanalytical collection of U–Pb, Lu–Hf and oxygen isotope data from zircon. The ability to collect such data individually has been around for 10–30 years, but only recently have these data been collected from the same spots, allowing synergy of interpretation. As an example, for magmatic zircons from an ore-related granite, the U–Pb system allows age determination (Chelle-Michou and Schaltegger 2023), the Lu–Hf system provides information about source of the magma (e.g. crustal versus mantle: Waltenberg 2023), and the oxygen system provides information about modifications of the source (e.g. metasomatism prior to magma generation: Valley 2003). Collectively, these data can provide information about the mineral system not available individually from the separate isotope information. For example, the data could indicate if a magma originated from the mantle and if the mantle had been metasomatized, potentially important information in determining magma fertility.

Another area with growth potential is the combination of isotope systems including the light stable isotopes described above (B, O, H, C, and S; also Li though not discussed herein), as well as heavier stable metal isotopes (e.g. Cu) and radiogenic isotopes. Many of these can be analysed in situ and with good precision by SIMS and/or LA-ICP-MS, which opens the door to detailed, petrographically-controlled analyses of zoning and overprinting relationships in ore and gangue minerals. Multiple-isotope analyses would remove much of the current ambiguity in identifying fluid and metals origin by isotope fingerprinting. However, a prerequisite for expanding the scope of in-situ analysis is the availability of homogeneous and matrix-matched reference materials for a wide range of mineral groups (oxides, sulfides, silicates, carbonates etc.). There needs to be heightened awareness of the importance for development and distribution of quality reference materials.

As discussed above and by Barker et al. (2013), the development of rapid, inexpensive methods of stable isotope data acquisition would enhance the utility of stable isotope data in mineral exploration. Although stable isotope data can provide vectors toward ore, the time required for analysis and the cost has generally restricted stable isotope (and other isotope) data to academic studies and not exploration. Continued development of rapid methods of analysis would increase the update by the exploration industry.

References

Adlakha EE, Hattori K, Davis WJ, Boucher B (2017) Characterizing fluids associated with the McArthur River U deposit, Canada, based on tourmaline trace element and stable (B, H) isotope compositions. Chem Geol 466:417–435

Aggerwal SK, You C-F (2016) A review on the determination of isotope ratios of boron with mass spectrometry. Mass Spec Rev 36:499–519

Akagi T, Franchi IA, Pillinger CT (1993) Oxygen isotope analysis of quartz by Nd/YAG-laser/ fluorination. Analyst (london) 118:1507–1510

Alirezaei S, Cameron EM (2001) Variations of sulfur isotopes in metamorphic rocks from Bamble Sector, southern Norway: a laser probe study. Chem Geol 181:23–45

Baksheev IA, Prokofiev VY, Trumbull RB, Wiedenbeck M, Yapaskurt VO (2015) Geochemical evolution of tourmaline in the Darasun gold district, Transbaikal region, Russia: evidence from chemical and boron isotopic compositions. Mineral Deposita 50:125–138

Barker SL, Dipple GM, Hickey KA, Lepore WA, Vaughan JR (2013) Applying stable isotopes to mineral exploration: teaching an old dog new tricks. Econ Geol 108:1–9

Barnes HL (ed) (1979) Geochemistry of hydrothermal ore deposits, 2nd edn. Wiley, New York, p 789

Barnes HL (ed) (1997) Geochemistry of hydrothermal ore deposits, 3rd edn. Wiley, New York, p 992

Barton LL, Fauque GD (2009) Biochemistry, physiology and biotechnology of sulfate-reducing bacteria. Adv Appl Microbiol 68:41–98

Bekker A, Barley ME, Fiorentini M, Rouxel OJ, Rumble D, Bersford SW (2009) Atmospheric sulfur in Archean komatiite-hosted nickel deposits. Science 326:1086–1089

Beaudoin G, Taylor BE (1994) high precision and spatial resolution sulfur isotope analysis using MILES laser microprobe. Geochim Cosmochim Acta 58:5055–5063

Beaudoin G, Therrien P (2009) The updated web stable isotope fractionation calculator. In: de Groot PA (ed) Handbook of stable isotope analytical techniques, vol II. Elsevier, Amsterdam, pp 1120–1122

Bendall C, Lahaye Y, Fiebig J, Weyer S, Brey GP (2006) In situ sulfur isotope analysis by laser ablation MC-ICPMS. Appl Geochem 21:782–787

Bigeleisen J, Perlman ML, Prosser HC (1952) Conversion of hydrogenic materials to hydrogen for isotope analysis. Anal Chem 24:1356–1357

Broecker W, Oversby V (1971) Chemical equilibria in the Earth. McGraw-Hill, New York, p 318

Burnham CW (1979) Magmas and hydrothermal fluids. In: Barnes HL (ed) Geochemistry of hydrothermal ore deposits, 2nd edn. Wiley, New York, pp 71–136

Caruso S, Fiorentini ML, Champion DC, Lu Y, Ueno Y, Smithies RH (2022) Sulfur isotope systematics of granitoids from the Yilgarn Craton sheds new light on the fluid reservoirs of Neoarchean orogenic gold deposits. Geochim Cosmochim Acta 326:199–213

Catanzaro EJ, Champion CE, Garner EL, Marinenko G, Sappenfield KM, Shields WR (1970) Boric acid; isotope, and assay standard reference materials. United States National Bureau of Standards Special Publication 260–17

Catling DC (2014) The great oxidation event transition. Treatise Geoch, 2nd edn 6:177–195. https://doi.org/10.1016/B978-0-08-095975-7.01307-3

Chacko T, Riciputi LR, Cole DR, Horita J (1999) A new technique for determining equilibrium hydrogen isotope fractionation factors using the ion microprobe: application to the epidote-water system. Geochim Cosmochim Acta 63:1–10

Chadwick J (1932) Possible existence of a neutron. Nature 129:312

Chelle-Michou C, Schaltegger U (2023) U-Pb dating of mineral deposits: from age constrains to ore-forming processes. In: Huston DL, Gutzmer J (eds) Isotopes in economic geology, metallogensis and exploration, Springer, Berlin, this volume

Clayton RN (2003) Oxygen isotopes in meteorites. Treatise Geoch 1:129–142

Clayton RN, Kieffer SW (1991) Oxygen isotope thermometer calibrations. Geochem Soc Spec Pub 3:3–10

Clayton RN, Mayeda TK (1963) The use of bromine pentafluoride in the extraction of oxygen from oxides and silicates for isotope analysis. Geochim Cosmochim Acta 27:43–52

Clayton RN, Grossman L, Mayeda TK (1973) A component of primitive nuclear composition in carbonaceous meteorites. Science 339:780–785

Clayton RN, Onuma N, Grossman L, Mayeda TK (1977) Distribution of the presolar component in allende and other carbonaceous chondrites. Earth Planet Sci Lett 34:209–224

Codeço MS, Weis P, Trumbull R, Glodny J, Wiedenbeck M, Romer RL (2019) Boron isotope muscovite-tourmaline geothermometry indicates fluid cooling during magmatic-hydrothermal W-Sn ore formation. Econ Geol 114:153–163

Cole DR, Ripley EM (1998) Oxygen isotope fractionation between chlorite and water from 170–350°C: a preliminary assessment based on partial exchange and fluid/rock experiments. Geochim Cosmochim Acta 63:449–457

Conrad R (2005) Quantification of methanogenic pathways using stable carbon isotope signatures: a review and a proposal. Org Geochem 36:739–752

Coplen TB (2011) Guideline and recommended terms for expression of stable-isotope-ratio and gas-ratio measurement results. Rapid Commun Mass Spectrom 25:2538–2560

Coplen TB, Kendall C, Hopple J (1983) Comparison of stable isotope reference samples. Nature 302:236–238

Craig H (1961) Isotope variations in meteoric waters. Science 133:1702–1703

Crowe DE, Valley JW, Baker KL (1990) Micro-analysis of sulfur-isotope ratios and zonation by laser microprobe. Geochim Cosmochim Acta 54:2075–2092

de Hoog JCM, Savov IP (2018) Boron isotopes as a tracer for subduction zone processes. Adv Isot Geochem 7:217–247

de Groot PA (ed) (2004) Handbook of stable isotope analytical techniques, vol 1. Elsevier, Amsterdam

de Groot PA (ed) (2009) Handbook of stable isotope analytical techniques, vol 2. Elsevier, Amsterdam

Detmers J, Brüchert V, Habicht KS, Juever J (2001) Divrsity of sulfur isotope fractionations by sulfate-reducing prokaryotes. Appl Environ Microbiol 2001:888–894

Ding T, Valkiers S, Kipphardt H, De Bièvre P, Taylor PDP, Gonfiantini R, Krouse R (2001) Calibrated sulfur isotope abundance ratios of three IAEA sulfur isotope reference materials and V-CDT with a reassessment of the atomic weight of sulfur. Geochim Cosmochim Acta 65:2433–2437

Ding X, Ripley EM, Shirey SB, Li C, Moore CH (2012) Os, Nd, O and S isotope constraints on the importance of country rock contamination in the generation of the conduit-related Eagele Ni-Cu-(PGE) deposit in the Midcontinent Rift System, Upper Michigan. Geochim Cosmochin Acta 89:10–30

Drivenes K, Larsen RB, Müller A, Sørensen BE, Wiedenbeck M, Raanes MP (2015) Late-magmatic immiscibility during batholith formation: assessment of B isotopes and trace elements in tourmaline from the land's end granite. SW England. Contrib Min Petrol 169:56. https://doi.org/10.1007/s00410-015-1151-6

Eagle RA, Tütken T, Martin TS, Tripati AK, Fricke HC, Connely M, Cifelli RL, Eiler JM (2011) Dinosaur body temperatures determined from isotope (^{13}C–^{18}O) ordering in fossil biominerals. Science 333:443–445

Eastoe CJ, Guilbert JM (1992) Stable chlorine isotopes in hydrothermal processes. Geochim Cosmochim Acta 56:4247–4255

Eiler JM (2007) "Clumped-isotope" geochemistry—the study of naturally-occurring, multiply-substituted isotopologues. Earth Planet Sci Lett 262:309–327

Eldridge CS, Compston W, Williams IS, Walshe JL, Both RA (1987) In situ microanalysis for $^{32}S^{34}S$ ratios using the ion microprobe SHRIMP. Intl J Mass Spectr Ion Proc 76:65–83

Eldridge DL, Guo W, Farquhar J (2016) Theoretical estimates of equilibrium sulfur isotope effects in aqueous sulfur systems: Highlighting the role of isomers in the sulfite and sulfoxylate systems. Geochim Cosmochim Acta 195:171–200

Elsenheimer D, Valley JW (1992) In situ oxygen isotope analysis of feldspar and quartz by Nd:YAG laser microprobe. Chem. Geol. (isotope Geoscience Section) 101:21–42

Engel AEJ, Clayton RN, Epstein S (1958) Variations in isotope composition of oxygen and carbon in Leadville Limestone (Mississippian, Colorado) and in its hydrothermal and metamorphic phases. J Geol 66:374–393

Engel AEJ, Engel CG (1958) Progressive metamorphism and granitization of the major paragneiss, NW Adirondack Mtns. N. y. Geol Soc Am Bull 69:1369–1413

Epstein S, Buchsbaum HA, Lowenstam H, Urey HC (1953) Revised carbonate-water isotope temperature scale. Geol Soc Am Bull 64:1315–1326

Farquhar J, Bao H, Thiemens M (2000) Atmospheric influence of Earth's earliest sulphur cycle. Science 289:756–758

Farquhar J, Savarino J, Airieau S, Thiemens MH (2001) Observation of wavelength sensitive mass-independent sulphur isotope effects during SO_2 photolysis: implications for the early atmosphere. J Geophys Res 106:1–11

Farquhar J, Peters M, Johnston DT, Strauss H, Masterson A, Wiechert U, Kaufman AJ (2007) Isotopic

evidence for Mesoarchaean anoxia and changing atmospheric sulphur chemistry. Nature 449:706

Ferry JM (1981) Petrology of graphitic sulfide-rich schists from south-central Maine: an example of desulfidation during prograde regional metamorphism. Am Mineral 66:908–931

Finch EG, Tomkins AG (2017) Pyrite-pyrrhotite stability in a metamorphic aureole: implications for orogenic gold genesis. Econ Geol 112:661–674

Fiorentini ML, Bekker A, Rouxel O, Wing BA, Maier W, Rumble D (2012) Multiple sulfur and iron isotope composition of magmatic Ni-Cu-(PGE) sulfide mineralization from eastern Botswana. Econ Geol 107:105–116

Foster GL, Hoenisch B, Paris G, Dwyer GS, Rae JWB, Elliott T, Gaillardet J, Hemming N, Louvat P, Vengosh A (2013) Interlaboratory comparison of boron isotope analyses of boric acid, seawater and marine $CaCO_3$ by MC-ICPMS and NTIMS. Chem Geol 358:1–14

Foster GL, Marschall HR, Palmer MR (2018) Boron isotope analysis of geological materials. Adv Isot Geochem 7:13–31

Friedman L, Lipman P, Obranovich JD, Gleason JD, Christiansen RL (1974) Meteoric waters in magmas. Science 184:1069–1072

Ghosh P, Adkins J, Affek H, Balta B, Guo W, Schauble EA, Schrag D, Eiler JM (2006) ^{13}C–^{18}O bonds in carbonate minerals: a new kind of paleothermometer. Geochim Cosmochim Acta 70:1439–1456

Giesemann A, Jäger HJ, Norman AL, Krouse HR, W.A. Brand WA, (1994) On-line sulfur-isotope determination using an elemental analyzer coupled to a mass spectrometer. Anal Chem 66:2816–2819

Gilg HA, Sheppard SMF (1996) Hydrogen isotope fractionation between kaolinite and water revisited. Geochim Cosmochim Acta 60:529–533

Goldhaber MB, Orr WL (1995) Kinetic controls on thermochemical sulfate reduction as a source of sedimentary H_2S. ACS Symp Ser 612:412–425

Graham CM, Sheppard SMF, Heaton THE (1980) Experimental hydrogen isotope studies: I. Systematics of hydrogen isotope fractionation in the systems epidote-H_2O, zoisite-H_2O and AlO(OH)-H_2O. Geochim Cosmochim Acta 44:353–364

Grinenko VA (1962) The preparation of sulphur dioxide for isotope analysis. Zh Neorgan Khim 7:2478–2483

Hagemann S, Hensler A-S, Figueiredo e Silva RC, Tsikos H (2023) Light stable isotope (O, H, C) signatures of BIF-hosted iron ore systems: implications for genetic models and exploration targeting. In: Huston DL, Gutzmer J (eds), Isotopes in economic geology, metallogensis and exploration, Springer, Berlin, this volume

Harder H (1974) 5D. Abundance in rock-forming minerals, boron minerals. In: Kedepohl KH (Ed) Handbook of geochemistry. Berlin, Springer Verlag, 5-D-1–5-D-6

Heidenreich JE III, Thiemens MH (1986) A non-mass dependent oxygen isotope effect in the production of

ozone from molecular oxygen: the role of molecular symmetry in isotope chemistry. J Chem Phys 84:2129–2136

Health Physics Society (2011) Tritium. Health Physics Society Fact Sheet. 5 p. http://hps.org/documents/tritium_fact_sheet.pdf

Hildreth W, Christiansen RL, O'Neil JR (1984) Catastrophic isotope modificatin of rhyolite magmas at times of caldera subsidence, Yellowstone Plateau volcanic field. J Geophys Res 89:10153–10192

Hoefs J (1997) Stable isotope geochemistry, 4th edn. Springer, Berlin, p 201

Hoefs J (2021) Stable isotope geochemistry, 9th edn. Springer, Berlin, p 504

Honlet R, Gasparrini M, Muchez P, Swennen R, John CM (2018) A new approach to geobarometry by combining fluid inclusion and clumped isotope thermometry in hydrothermal carbonates. Terra Nova 2018:1–8. https://doi.org/10.1111/ter.12326

Horita J, Wesolowski DJ (1994) Liquid-vapor fractionation of oxygen and hydrogen isotopes of water from the freezing to the critical temperature. Geochim Cosmochim Acta 58:3425–3437

Hulston JR, Thode HG (1965) Variations in S^{33}, S^{34}, and S^{36} contents of meteorites and their relation to chemical nuclear effects. J Geophys Res 70:3475–3484

Huntington KW, Budd DA, Wernicke BP, Eiler JM, JM, (2011) Use of clumped-isotope thermometry to constrain the crystallization temperature of diagenetic calcite. J Sed Res 81:656–669

Huston DL, Champion DC (2023) Applications of lead isotopes to ore geology, metallogenesis and exploration. In: Huston DL, Gutzmer J (eds), Isotopes in economic geology, metallogensis and exploration, Springer, Berlin, this volume

Huston DL, Bolger C, Cozens G (1993) A comparison of mineral deposits at the Gecko and White Devil deposits: implications for ore genesis in the Tennant Creek district, Northern Territory, Australia. Econ Geol 88:1198–1225

Huston DL, Relvas JMRS, Gemmell JB, Drieberg S (2011) The role of granites in volcanic-hosted massive sulphide ore-forming systems: an assessment of magmatic–hydrothermal contributions. Mineral Deposita 46:473–507

Huston DL, LaFlamme C, Beaudoin G, Piercey S (2023) Light stable isotopes in volcanic-hosted massive sulfide ore systems. In: Huston DL, Gutzmer J (eds), Isotopes in economic geology, metallogensis and exploration, Springer, Berlin, this volume

Ireland TR (1995) Ion microprobe mass spectrometry: techniques and applications in cosmochemistry, geochemistry, and geochronology. Adv Anal Geochem 2:1–118

Ireland TR (2012) Oxygen isotope tracing of the solar system. Austr J Earth Sci 59:225–236

Ireland TR, Schram N, Holden P, Lanc P, Ávila J, Armstrong R, Amelin Y, Latimore A, Corrigan D, Clement S, Foster J, Compston W (2014) Charge-

mode electrometer measurements of S-isotopic compositions on SHRIMP-SI. Int J Mass Spectrometry 359:26–37

Jia Y, Kerrich R (1999) Nitrogen isotope systematics of mesothermal lode gold deposits: metamorphic, granitic, meteoric water, or mantle origin? Geology 27:1051–1054

Johnston DT (2011) Multiple sulfur isotopes and the evolution of Earth's surface sulfur cycle. Earth Sci Rev 106:161–183

Kelley SP, Fallick AE (1990) High precision spatially resolved analysis of $\delta^{34}S$ in sulphides using a laser extraction technique. Geochim Cosmochim Acta 54:883–888

Kennedy CB, Gault AG, Fortin D, Clark ID, Pedersen K, Scott SD, Ferris FG (2010) Carbon isotope fractionation by circumneutral iron-oxidizing bacteria. Geology 38:1087–1090

Kerrich R (1987) The stable istoope geochemistry of Au-Ag vein deposits in metamorphic rocks. Mineral Assoc Can Short Course Handb 13:287–336

Kharaka YK, Hanor JS (2003) Deep fluids in the continents: I. Sedimentary Basins. Treatise Geochem 5:1–48. https://doi.org/10.1016/B0-08-043751-6/05085-4

Kieffer SW (1982) Thermodynamics and lattice vibration of minerals: 5. Application to phase equilibria, isotope fractionation, and high pressure thermodynamic properties. Rev Geophys Space Phys 20:827–849

Kita NT, Ushikubo T, Fu B, Valley JW (2009) High precision SIMS oxygen isotope analysis and the effect of sample topography. Chem Geol 264:43–57

Kita NT, Huberty JM, Kozdon R, Beard BL, Valley JW (2010) High-precision SIMS, sulfur and iron stable isotope analyses of geological materials: accuracy, surface topography and crystal orientation. Surf Interface Anal 2010. https://doi.org/10.1002/sia.3424

Konrad-Schmolke M, Halama R (2014) Combined thermodynamic–geochemical modeling in metamorphic geology: Boron as tracer of fluid–rock interaction. Lithos 208–209:393–414

Korff SA, Danforth WE (1939) Neutron measurements with boron-trifluoride counters. Phys Rev 55:980

Kowalski P, Wunder B (2018) Boron-isotope fractionation among solids-fluids-melts: experiments and atomic modelling. Adv Isot Geochem 7:33–70

Kyser TK, ed (1987) Stable isotope geochemistry of low temperature fluids. Min Assoc Can Short Course 13

Kyser K (1986) Stable isotope variations in the mantle. Rev Mineral 16:141–164

LaFlamme C, Fiorentini ML, Lindsay MD, Bui TH (2018a) Atmospheric sulfur is recycled to the crystalline continental crust during supercontinent formation. Nature Commun 9:4380

LaFlamme C, Sugiono D, Thébaud N, Caruso S, Fiorentini M, Selvaraja V, Jeon H, Voute F, Martin L (2018b) Multiple sulfur isotopes monitor fluid evolution of an Archean orogenic gold deposit. Geochim Cosmochim Acta 222:436–446

Lambert-Smith JS, Rocholl A, Treloar PJ, Lawrence DM (2016) Discriminating fluid source regions in orogenic gold deposits using B-isotopes. Geochim Cosmochim Acta 194:57–76

Large RR (1975) Zonation of hydrothermal minerals at the Juno mine, Tennant Creek goldfield, central Australia. Econ Geol 70:1387–1413

Lesher CM, Campbell IH (1993) Geochemical and fluid dynamic modeling of compositional variations in Archean komatiite-hosted nickel sulfide ores in Western Australia. Econ Geol 88:804–816

Li YB, Liu JM (2006) Calculation of sulfur isotope fractionation in sulfides. Geochim Cosmochim Acta 70:1789–1795

Lloyd MK, Eiler JM, JM, Peter I. Nabelek PI, (2017) Clumped isotope thermometry of calcite and dolomite in a contact metamorphic environment. Geochim Cosmochim Acta 197:323–344

Lobato LM, Figueiredo e Silva RC, Angerer T, Mendes M, Hagemann S (2023) Fe isotopes applied to BIF-hosted iron ore deposits. In: Huston DL, Gutzmer J (eds), Isotopes in economic geology, metallogensis and exploration, Springer, Berlin, this volume

Lyons T (2007) Mass-independent fractionation of sulfur isotopes by isotope-selective photodissociation of SO_2. Geophys Res Lett 34:L22811

Machel HG (2001) Bacterial and thermochemical sulfate reduction in diagenetic environments – old and new insights. Sed Geol 140:143–175

Machel HG, Krause HR, Sassen R (1995) Products and distinguishing criteria of bacterial and thermochemical sulfate reduction. Appl Geochem 10:373–389

Marschall HR, Jiang S-Y (2011) Tourmaline isotopes: no element left behind. Elements 7:313–319

Marschall HR, Meyer C, Wunder B, Ludwig T, Heinrich W (2009) Experimental boron isotope fractionation between tourmaline and fluid: confirmation from in situ analyses by secondary ion mass spectrometry and from Rayleigh fractionation modelling. Contrib Mineral Petrol 158:675–681

Marschall HR, Foster GL (2018) Boron isotopes - the fifth element. Advances in Geochemistry 7:249–272

Mason PR, Košler J, de Hoog JC, Sylvester PJ, Meffan-Main S (2006) In situ determination of sulfur isotopes in sulfur-rich materials by laser ablation multiple-collector inductively coupled plasma mass spectrometry (LA-MC-ICP-MS). J Anal at Spectrom 21:177–186

Mathur R, Zhao Y (2023a) Copper isotopes used in mineral exploration. In: Huston DL, Gutzmer J (eds), Isotopes in economic geology, metallogensis and exploration, Springer, Berlin, this volume

Mauersberger K (1987) Measurement of heavy ozone in the stratosphere. Geophys Res Lett 8:80–83

McCrea JM (1950) On the isotope chemistry of carbonates and a paleotemperature scale. J Chem Phys 18:849–857

McKinney CR, McCrea JM, Epstein S, Allen HA, Urey HC (1950) Improvements in mass spectrometers for the measurement of small differences in isotope abundance ratios. Rev Sci Instrum 21:724–730

Mercadier J, Richard A, Cathelineau M (2012) Boron- and magnesium-rich marine brines at the origin of giant unconformity-related uranium deposits: $\delta^{11}B$ evidence from Mg-tourmalines. Geology 40:231–234

Mering JA, Barker SLL, Huntington KW, Simmons S, Dipple G, Andrew B, Schauer A (2018) Taking the temperature of hydrothermal ore deposits using clumped isotope thermometry. Econ Geol 113:1671–1678

Meshoulan A, Ellis GS, Ahmad WS, Deev A, Sessions AL, Yang Y, Adkins JF, Liu J, Gilhooly WP III, Aizenshtat Z, Amrani A (2016) Study of thermochemical sulfate reduction mechanism using compound specific sulfur isotope analysis. Geochim Cosmochim Acta 188:73–92

Mikova J, Kosler J, Wiedenbeck M (2014) Matrix effects during laser ablation MC ICP-MS analysis of boron isotopes in tourmaline. J Anal at Spectrom 29:903–914

Miller C, Halley S, Green G, Jones M (2001) Discovery of the West 45 volcanic-hosted massive sulfide deposit using oxygen isotopes and REE geochemistry. Econ Geol 96:1227–1238

Moran AE, Sisson VB, Leeman WP (1992) Boron depletion during progressive metamorphism: implications for subduction processes. Earth Planet Sci Lett 111:331–349

Muehlenbachs K, Anderson AT Jr, Sigvaldason GE (1974) Low O-18 basalts from Iceland. Geochim Gosmoshim Acta 38:577–588

Nabelek PI, Labotka C, O'Neil JR, Papike JJ (1984) Contrasting fluid/rock interaction between the Notch Peak granitic intrusion and argillites and limestones in western Utah: Evidence from stable isotopes and phase assemblages. Contrib Mineral Petrol 86:25–34

Naito K, Fukahori Y, He P, Sakurai W, Shimazaki H, Matsuhisa Y (1995) Oxygen and carbon isotope zonations of wall rocks around the Kamioka Pb-Zn skarn deposits, central Japan: application to prospecting. J Geochem Explor 54:199–211

Nier AO (1937) A mass-spectrographic study of the isotopes of Hg, Xe, Kr, Be, I, As, and Cs. Phys Rev 52:933

Ohmoto H (1972) Systematics of sulfur and carbon isotopes in hydrothermal ore deposits. Econ Geol 67:551–579

Ohmoto H (1986) Stable isotope geochemistry of ore deposits. Rev Mineral 16:491–559

Ohmoto H, Goldhaber RO (1997) Sulfur and carbon isotopes. In: Barnes HL (ed) Geochemistry of hydrothermal ore deposits, 2nd edn. Wiley, New York, pp 517–612

Ohmoto H, Lasaga AC (1982) Kinetics of reactions between aqueous sulfate and sulfides in hydrothermal systems. Geochim Cosmochim Acta 46:1727–1745

Ohmoto H, Rye RO (1979) Isotopes of sulfur and carbon. In: Barnes HL (ed) Geochemistry of hydrothermal ore deposits, 2nd edn. Wiley, New York, pp 509–567

Pack A, Herwartz D (2014) The triple oxygen isotope composition of the Earth mantle and understanding $\Delta^{17}O$ variations in terrestrial rocks and minerals. Earth Planet Sci Lett 390:138–145

Pal DC, Trumbull R, Wiedenbeck M (2010) Chemical and boron isotope compositions of tourmaline from the Jaduguda U (-Cu-Fe) deposit, Singhbhum shear zone, India: implications for the source and evolution of the mineralizing fluid. Chem Geol 277:245–260

Palmer MR, Slack JF (1989) Boron isotope composition of tourmaline from massive sulfide deposits and tourmalinites. Contrib Mineral Petrol 103:434–451

Paterson BA, Riciputi LR, McSween HY Jr (1997) A comparison of sulfur isotope ratio measurement using two ion microprobe techniques and application to analysis of troilite in ordinary chondrites. Geochim Cosmochim Acta 61:601–609

Peters ST, Alibabaie N, Pack A, McKibbin SJ, Raeisi D, Nayebi N, Torab F, Ireland T, Lehmann B (2020) Triple oxygen isotope variations in magnetite from iron-oxide deposits, central Iran, record magmatic fluid interaction with evaporite and carbonate host rocks. Geology 48:211–215

Phillips GN, Groves DI (1983) The nature of Archaean gold-bearing fluids as deduced from gold deposits in Western Australia. J Geol Soc Austr 30:25–39

Pichlmayer F, Blochberger K (1988) Isotopenhäufigkeitsanalyse von kohlenstoff, stickstoff und schwefel mittels gerätekopplung elementaranalysator-massenspektrometer. Fresenius' Zeitschrift Für Analytische Chemie 331:196–201

Pitcairn IK, Olivo GR, Teagle DAH, Craw D (2010) Sulfide evolution during prograde metamorphism of the Otago and Alpine schists. Can Mineral 48:1267–1295

Puchelt H, Sabels BR, Hoering TC (1971) Preparation of sulfur hexafluoride for isotope geochemical analysis. Geochim Cosmochim Acta 35:625–628

Quesnel B, Scheffer C, Beaudoin G (2023b) The light stable isotope (H, B, C, N, O, Si, S) composition of orogenic gold deposits. In: Huston DL, Gutzmer J (eds), Isotopes in economic geology, metallogensis and exploration, Springer, Berlin, this volume

Rafter TA (1957) Sulphur isotope variations in nature. Part I-the preparation of sulphur dioxide for mass spectrometer examination. NZ J Sci Technol 838:849–857

Robinson BS, Kusakabe M (1975) Quantitative preparation of sulfur dioxide, for $^{34}S/^{32}S$ analyses, from sulfides by combustion with cuprous oxide. Anal Chem 47:1179–1181

Rosman KJR, Taylor PDP (1998) Isotope composition of the elements 1997. Pure Appl Chem 70:217–235

Rotherham J, Blake KL, Cartwright I, Williams P (1998) Stable isotope evidence for the origin of the Mesoproterozoic Starra Au-Cu deposit, Cloncurry District, Northwest Queensland. Econ Geol 93:1435–1449

Rumble D, Hoering TC, Palin JM (1993) Preparation of SF_6 for sulfur isotope analysis by laser heating sulfide minerals in the presence of F_2 gas. Geochim Cosmochim Acta 57:4499–4512

Rye RO (2005) A review of the stable-isotope geochemistry of sulfate minerals in selected igneous environments and related hydrothermal systems. Chem Geol 215:5–36

Rye RO, Bethke PM, Wasserman MD (1992) The stable isotope geochemistry of acid sulfate alteration. Econ Geol 87:225–262

Sah RH, Brown PH (1997) Boron determination — a review of analytical methods. Microchem J 56:285–304

Sasaki A, Arilawa Y, Folinsbee RE (1979) Kiba reagent method of sulfur extraction applied to isotope work. Bull Geol Surv Japan 30:241–245

Schmitt AK, Simon JI (2004) Boron isotope variations in hydrous rhyolitic melts - a case study from Long Valley, California. Contrib Mineral Petrol 146:590–605

Seal RR II (2006) Sulfur Isotope Geochemistry of Sulfide Minerals: Rev Mineral 61:633–677

Shanks WC III (2014) Stable isotope geochemistry of mineral deposits. Treatise Geochem, 2nd edn 13:59–85. https://doi.org/10.1016/B978-0-08-095975-7.01103-7

Sharp ZD (1990) A laser-based microanalytical method for the in situ determination of oxygen isotope ratios of silicates and oxides. Geochim Cosmochim Acta 54:1353–1357

Sharp ZD, Gibbons JA, Maltsev O, Atudorei V, Pack A, Sengupta S, Shock EL, Knauth LP (2016) A calibration of the triple oxygen isotope fractionation in the SiO_2-H_2O system and applications to natural samples. Geochim Cosmochim Acta 186:105–119

Sheppard SMF, Nielsen RL, Taylor HP Jr (1969) Oxygen and hydrogen isotope ratios of clay minerals from porphyry copper deposits. Econ Geol 64:755–777

Sheppard SMF, Nielsen RL, Taylor HP Jr (1971) Hydrogen and oxygen isotope ratios in minerals from porphyry copper deposits. Econ Geol 66:515–542

Sheppard SMF (1986) Characterization and isotope variations in natural waters. Rev Mineral 16:165–184

Shimizu N, Hart SR (1982) Isotope fractionation in seeondary ion mass spectrometry. J Appl Phys 53:1303–1311

Siegel K, Wagner T, Trumbull RB, Jonsson E, Matalin G, Wälle M, Heinrich CA (2016) Stable isotope (B, H, O) and mineral-chemistry constraints on the magmatic to hydrothermal evolution of the Varutrask rare-element pegmatite (northern Sweden). Chem Geol 421:1–16

Simmons SF, Sawkins FJ, Schlutter DJ (1987) Mantle-derived helium in two Peruvian hydrothermal ore deposits. Nature 329:429

Simmons SF, White NC, John DA (2005) Geological characteristics of epitherm precious and base metal deposits. Econ Geol 100th Anniv Vol, p 485–522

Slack JF, Trumbull RB (2011) Tourmaline as a recorder of ore-forming processes. Elements 7:321–326

Soddy F (1913) Intra-atomic charge. Nature 92:399–400

Swanson EM, Wernicke BP, Eiler JM, Losh S (2012) Temperatures and fluids on faults based on carbonate clumped isotope thermometry. Am J Sci 312:1–21

Taylor HP Jr (1979) Oxygen and hydrogen isotope relationships in hydrothermal mineral deposits. In: Barnes HL (ed) Geochemistry of hydrothermal ore deposits, 2nd edn. Wiley, New York, pp 236–277

Taylor BE (1986a) Magmatic volatiles: isotope variation of C, H and S. Rev Mineral 16:185–225

Taylor HP Jr (1986b) Igneous rocks: II. Isotope case studies of circumpacific magmatism. Rev Mineral 16:273–318

Taylor BE (1987) Stable isotope geochemistry of ore-forming fluids. Mineral Assoc Can Short Course Handb 13:337–445

Taylor HP Jr (1997) Oxygen and hydrogen isotope relationships in hydrothermal mineral deposits. In: Barnes HL (ed) Geochemistry of hydrothermal ore deposits, 3rd edn. Wiley, New York, pp 229–302

Taylor HP Jr, Sheppard SMF (1986) Igneous rocks: 1. Processes of isotope fractionation and isotope systematics. Rev Mineral 16:227–272

Thode HG, Monster J, Durford HB (1961) Sulphur Isotope Geochemistry. Geochim Cosmochi Acta 25:159–174

Thom J, Anderson GM (2008) The role of thermochemical sulfate reduction in the origin of Mississippi Valley-type deposits. I. Experimental Results. Geofluids 8:16–26

Thomson JJ (1913) Rays of positive electricity. Proc Royal Soc A 89:1–20

Trumbull RB, Slack JF (2018) Boron isotopes in the continental crust: granites, pegmatites, felsic volcanic rocks and related ore deposits. Advances in Geochemistry 7:249–272

Trumbull RB, Codeco MS, Jiang S-Y, Palmer MR, Slack JF (2020) Application of boron isotopes in tourmaline to understanding hydrothermal ore systems. Ore Geol Rev 125:103682

Ueno Y, Johnson MS, Danielache SO, Eskebjerg C, Pandey A, Yoshida N (2009) Geological sulfur isotopes indicate elevated OCS in the Archean atmosphere, solving faint young sun paradox. Proc Natl Acad Sci USA 106:14784–14789

Ueno Y, Aoyama S, Endo Y, Matsu'ura F, Foriel J, (2015) Rapid quadruple sulfur isotope analysis at the sub-micromole level by a flash heating with CoF_3. Chem Geol 419:29–35

Urey HC (1947) The thermodynamics of isotope substances. J Chem Soc 1947:562–581

Valley JW (1986) Stable isotope geochemistry of metamorphic rocks. Rev Mineral 16:445–490

Valley JW (2003) Oxygen isotope in zircon. Rev Mineral 53:343–385

Valley JW, Cole D, eds (2001) Stable isotope geochemistry. Rev Mineral 43:531 p

Valley JW, Graham CM (1991) Ion microprobe analysis of oxygen isotope ratios in metamorphic magnetite-diffusion reequilibration and implications for thermal history. Contr Mineral Petrol 109:38–52

Valley JW, Taylor Jr HP, O'Neill JR, eds (1986) Stable isotopes in high temperature geological processes. Rev Mineral 16:570 p

Vennemann TW, O'Neil JR (1993) A simple and inexpensive method of hydrogen isotope and water analyses of minerals and rocks based on zinc reagent. Chem Geol (isot Geosci Sect) 103:227–234

Waltenberg K (2023) Application of Lu-Hf isotopes to ore geology, metallogenesis and exploration. In: Huston DL, Gutzmer J (eds), Isotopes in economic geology, metallogensis and exploration, Springer, Berlin, this volume

Wedepohl KH (1969a) Compositon and abundance of common sedimentary rocks. In: Wedepohl KD (ed) Handbook of geochemistry. Springer-Verlag, New York, pp 250–271

Wedepohl KH (1969b) Compositon and abundance of common igneous rocks. In: Wedepohl KD (ed) Handbook of geochemistry. Springer-Verlag, New York, pp 227–249

Werner RA, Brand WA (2001) Referencing strategies and techniques in stable isotope ratio analysis. Rapid Commun Mass Spectrom 15:501–519

Whitehouse MJ (2013) Multiple sulfur isotope determination by SIMS: evaluation of reference sulfides for Δ^{33}S with observations and a case study on the determination of Δ^{36}S. Geostand Geoanal Res 37:19–33

Whiticar MJ (1999) Carbon and hydrogen isotope systematics of bacterial formation and oxidation of methane. Chem Geol 161:291–314

Williams N (2023) Light-element stable isotope studies of the clastic-dominated lead-zinc mineral systems of northern Australia & the North American Cordillera: implications for ore genesis and exploration. In: Huston DL, Gutzmer J (eds) Isotopes in economic geology, metallogensis and exploration, Springer, Berlin, this volume

Wilkinson JJ (2023) The potential of Zn isotopes in the science and exploration of ore deposits. In: Huston DL, Gutzmer J (eds) Isotopes in economic geology, metallogensis and exploration, Springer, Berlin, this volume

Xavier RP, Wiedenbeck M, Trumbull RB, Dreher AM, Monteiro LVS, Rhede D, de Araújo CEG, Torresi I (2008) Tourmaline B-isotopes fingerprint marine evaporites as the source of high salinity ore fluids in iron oxide-copper-gold deposits, Carajás Mineral Province (Brazil). Geology 36:743–746

Young ED, Galy A, Nagahara H (2002) Kinetic and equilibrium mass-dependent isotope fractionation laws in nature and their geochemical and cosmochemical significance. Geochim Cosmochim Acta 66:1095–1104

Zheng Y-F (1993a) Calculation of oxygen isotope fractionation in anhydrous silicate minerals. Geochim Cosmochim Acta 57:1079–1091

Zheng Y-F (1993b) Calculation of oxygen isotope fractionation in hydroxyl-bearing silicates. Earth Planet Sci Lett 120:247–263

Zheng Y-F (1999) Oxygen isotope fractionation in carbonate and sulfate minerals. Geochem J 33:109–126

Zheng YF, Simon K (1991) Oxygen isotope fractionation in hematite and magnetite: a theoretical calculation and application to geothermometry of metamorphic iron-formation. Eur J Mineral 3:877–886

Zhong R, Brugger J, Tomkins AG, Chen Y, Li W (2015) Fate of gold and base metals during metamorphic devolatilization of a pelite. Geochim Cosmochim Acta 171:338–352

Zhou T, Yuan F, Yue S, Liu X, Zhang X, Fan Y (2007) Geochemistry and evolution of ore-forming fluids of the Yueshan Cu–Au skarn-and vein-type deposits, Anhui Province, South China. Ore Geol Rev 31:279–303